Isoindigo dyes functionalized with terminal electron-withdrawing groups: Computational, optical and electrical characterization

Isoindigo dyes functionalized with terminal electron-withdrawing groups: computational, optical and electrical characterization

Antonio Carella,[a*] Marcello Franzini, [a,b] Sandra Fusco, [a] Roberto Centore, [a] Mario Barra, [c] Fabio Chiarella, [c] Antonio Cassinese, [c,d] Matteo Bonomo, [b] Stefano Nejrotti, [b] Marilena Carbone, [e] Lorenzo Gontrani. [e]

a) Dipartimento di Scienze Chimiche, Università degli Studi di Napoli 'Federico II', Complesso Universitario Monte Sant'Angelo, Via Cintia 21, I-80126 Napoli, Italy; b) Department of Chemistry and NIS Interdepartmental Centre, University of Torino, Via Pietro Giuria 7, 10125 Torino, Italy; c) CNR-SPIN, c/o Dipartimento di Fisica "Ettore Pancini", P.le Tecchio, 80, I-80125 Napoli, Italy; d) Dipartimento di Fisica "Ettore Pancini", P.le Tecchio, 80, I-80125 Napoli, Italy; e) Dipartimento di Scienze e Tecnologie Chimiche, Università di Roma "Tor Vergata", Via della ricerca scientifica 1, I-00133 Roma, Italy.

*Corresponding author: antonio.carella@unina.it

Abstract

Eight novel isoindigo (**iI**) based small molecules have been successfully synthesized. Their molecular structure consists of an electron acceptor **iI** core symmetrically linked to two furan (F-series) or thiophene (T-series) rings and end-functionalized with four auxiliary electron withdrawing groups (EWGs) of different strength. The optical properties of the dyes in chloroform solution are uniformly modulated by the terminal EWGs so that absorption maxima wavelengths move to higher values as the EWG's strength increases. A computational (DFT level) analysis provides useful information on the electronic structure of the dyes: upon photoexcitation the electron density moves away from **iI** core or towards it according to the different EWG considered.

Optical analysis is performed on dyes' thin films as well and a general broadening and red shift of the absorption is observed as compared to the behaviour in solution; all the dye's thin films are characterized by narrow bandgaps (< 1.60 eV) and diffused absorption of most of the visible light. From XRD diffraction analysis performed on drop casted films of the dyes, it is possible to observe a lamellar organization in the solid phase with lamellae width clearly linked to the nature of the terminal EWG. HOMO and LUMO energies of the dyes, determined by cyclic voltammetry analysis performed on dyes' thin films, show very stable LUMO and HOMO energy levels, suggesting, respectively, a tendency to act as n-type semiconductors and a very good thermo-oxidative stability. The dyes are finally employed as active layers in organic field effect transistors to study their charge transport properties: all of them display unipolar n-type charge transport with the presence of the electron accumulation phenomenon under the application of positive gate voltages. For one of the dye, mobility (μ) up to 10^{-2} $cm^2/V{\cdot}s$ was measured, whereas values around 10^{-3} $cm^2/V{\cdot}s$ were found for the others.

Keywords: synthesis, isoindigo, DFT, organic electronics, n-type semiconductors.

1. Introduction

The world of industrial dyes and pigments has provided several π-conjugated scaffolds for useful application in the field of organic electronics[1] such as, for instance, perylene tetracarboxylic acid di-imides (PDI)[2,3] or diketopyrrolopyrrole (DPP) derivatives.[4–6] In this context, indigoids represent a very important class of natural pigments, based on the connection between two indole moieties.[7] The most important of these pigments, indigo (see Scheme 1), played a fundamental role in the history of pigments with its first use dating back at least to 2000 BC: it was (along with its 6,6'-dibromo-derivative known as Tyrian purple) the only blue dye that could be exploited to colour textiles. Lately, in the 19th century, the quest for producing dyestuff at a more affordable

cost, prompted the development of synthetic organic chemistry and the growth of the main chemical companies still existing nowadays, and to this regard the study of indigo chemistry engaged the best organic chemists of that period.[8] Isoindigo (**iI**), characterized by a less appealing brown colour, is a naturally occurring isomer of indigo extracted as minor component from the mixture of indigoid dyes found in the leaves of *isatis tinctoria* (see Scheme 1).

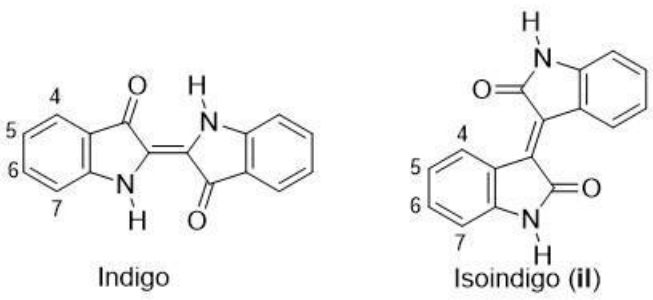

Scheme 1. Indigo and isoindigo molecular structure

Though **iI** was somehow less interesting than the most famous isomer when used as classical pigment, its derivatives are gaining a growing success in the field of organic semiconductors (OSCs):[8–12] **iI** features a highly planar structure, characterized by a strong electron-acceptor character due to the presence of the two lactamic units. It is synthesized quantitatively by a simple condensation between isatin and oxindole in acetic acid, catalysed by HCl. The large availability of several commercial derivatives of both isatin and oxindole allows for the preparation of a wide range of **iI**-based compounds. Unlike in indigo, the nitrogen of the ring is not involved in an intramolecular hydrogen bond with carbonyl group and can be readily alkylated, permitting the synthesis of soluble derivatives. Moreover, a further extension of the conjugation can be achieved by C-C cross coupling reactions, in particular at 6,6’ positions of the phenyl rings. This synthetic versatility led to the employment of **iI** as building block in the preparation of a wide variety of derivatives: several donor-acceptor polymers where the electron acceptor **iI** unit was polymerized with electron donor moieties are reported in the literature showing excellent performance both in

the field of organic photovoltaics[13–15] and organic transistors.[16–18] **iI**-containing small molecules for organic electronics have been instead less extensively investigated than polymeric counterparts. Nevertheless, in the last few years a growing interest towards the use of small molecules OSCs has been reported:[19,20] molecular systems exhibit, indeed, some advantages, as a higher reproducibility; moreover, a thoughtful molecular engineering design allows to finely tune both electronic properties and structural packing. In the context of small molecule OSCs, we recently proposed novel dyes containing the well-known diketopyrrolopyrrole (**DPP**) electron acceptor moiety; the molecular architecture of these materials was based on a **DPP**-core symmetrically flanked with electron-donor groups (bifurane[21] or bithiophene[22]) and end capped with auxiliary electron-withdrawing groups (EWGs). A significant absorption in the NIR zone of the spectrum and appealing ambipolar charge transport properties were the key properties of these compounds; they were synthesized through a modular approach that allows designing new materials by simply changing the nature of the three basic constituents of the molecular structure (acceptor core, donors, terminal EWGs). In this work, we explore the effect of replacing the DPP electron-acceptor core with **iI** group. The chemical structures of the new dyes are shown in Scheme 2. It is possible to classify the prepared dyes into two groups, namely T- and F-series. In each series, the derivatives are characterized by a common molecular fragment consisting of a central **iI** unit, symmetrically linked to two electron-donor units (furan rings in F-series thiophene rings in T-series). The molecules differ for the terminal groups, consisting of four different auxiliary electron-acceptor units: dicyanovinyl (**DCV**), N,N'-diethylthiobarbituric acid (**TB**), indandione (**ID)** and 1,1-dicyanomethylene-3-Indanone **(IDM**). The use of auxiliary EWGs with different strengths was designed to modulate the absorption and electronic properties of the molecules, as already observed in previous works by some of us.[23,24] The **iI** core is

functionalized on lactam nitrogen with 2-octyldodecyl groups, with the aim of increasing the solubility of the molecules.

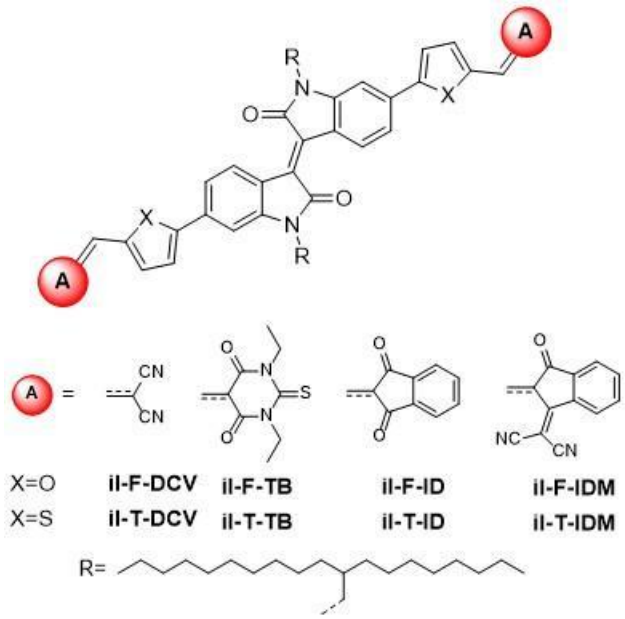

Scheme 2. General molecular formulas of the synthesized dyes

Previous works based on comparison between A-D polymers containing DPP or **iI** as acceptor units, show a significant stabilization of frontier molecular orbitals when **iI** is used.[25,26] The idea that motivated this study was that, upon stabilization of LUMO and HOMO orbitals, it could be possible to turn the ambipolar charge transport behaviour shown by the previous **DPP**-based in dyes in a pure n-type behaviour and to improve the thermo-oxidative stability as well. The synthesized dyes have been thoroughly characterized regarding their thermal, optical, structural, electrochemical properties. A scrupulous theoretical investigation performed at DFT level was carried out to shed light on the electronic structures of the dyes and to highlight the differences with the previously reported parent DPP molecules. The dyes were finally processed as thin films and used as active layers in organic field effect transistors (OFET) to investigate their charge transport properties.

2. Experimental

2.1. Materials and chemical physical characterization

All reagents were purchased by Sigma Aldrich, AlfaAesar or Fluorochem and used without any further purification. All air- or moisture-sensitive reactions were carried out under nitrogen atmosphere. 6,6'-dibromoisoindigo and 1-bromo-2-octyldodecane were synthesized according to reported procedures. [22,27] Details of the synthetic procedures are reported in detail in the following. The compounds' identity was confirmed by Bruker Avance 400 MHz, Varian Inova 500 MHz and Jeol ECZR600 MHz NMR spectrometers. Mass spectra were recorded with a MALDI-TOF-TOF 5800 Ab Sciex instrument (reflector positive ion mode). Thermogravimetric analysis (TGA) was carried by a TA4000 Perkin- Elmer instrument at a heating rate of 20 °C min^{-1} under air in the temperature range 30-900 °C. The reported decomposition temperature refers to 5% weight loss. Differential scanning calorimetry (DSC) analysis was performed on a DSC Mettler 822e instrument under a nitrogen flow at a heating rate of 10 °C min^{-1}. Absorption spectra were recorded on Jasco V-530 UV-vis spectrophotometer at room temperature with a scanning rate of 200 nm/min. FTIR spectra were recorded dispersing the dye in KBr pellets and using a Thermofisher Nicolet 5700 FTIR spectrometer. Thin films of the dyes for optical characterization were prepared by spin-coating a $CHCl_3$/1,1-2,2-tetrachloroethane (TCE) 95/5 v/v solution (5 mg/ml) of the dyes on glass substrates by means of a Laurell WS-650Mz-23NPP spin processor. Electrochemical characterization was performed by cyclic voltammetry (CV) using a BioLogic sp150. Some attempts were made to characterize the dye in solution (0.1M tetrabutylammoiun hexafluorophosphate in dichloromethane) but they failed due to the limited solubility of the samples. Therefore, we resolved to solid-state analyses in a three-electrode set-up: the samples were drop-casted from supersaturated dichloromethane (DCM) solution onto a platinum disc acting as working electrode, whereas a Pt wire and Ag/AgCl(3M) were exploited as counter-electrode and reference electrode, respectively. Electrolyte consisted in a

tetrabutylammonium hexafluorophosphate 0.1M solution in anhydrous acetonitrile. CV were conducted at 100 mV/s. The found potential values were referred to Fc/Fc+ acting as internal standard. Before each measurement, the electrolyte was degassed with Argon to avoid the presence of oxygen. For XRD analysis, thin films of the dyes were obtained by drop casting a 10 mg/ml $CHCl_3$ solution on a coverslip microscope glass and annealed for 1 h at 120 °C: their X-ray diffraction profiles were obtained with a Philips PW1830 powder diffractometer, using Cu Kα radiation (λ =1.5418 Å), by a continuous scan of the diffraction angle 2θ at a speed of 0.01°/s.

2.2. Synthetic procedures.

Synthesis of (*E*)-6,6'-dibromo-1,1'-bis(2-octyldodecyl)-[3,3'-biindolinylidene]-2,2'-dione (iI-OD-Br_2)

3.0 g (7.14 mmol) of iI-Br_2 and 3.0 g (0.0215 mol) K_2CO_3 were added to a reaction flask containing 50 mL of anhydrous DMF. Three nitrogen vacuum cycles were carried out, and then the temperature was raised to 110 °C and after 40 minutes, 6.0 g (0.01714) mol of 1-bromo-2-octyldodecane were added. The reaction was kept overnight at 110 °C. Then, the solution was left to cool down at room temperature and extracted with brine and dichloromethane (1:1). The organic phase was then treated with a rotary evaporator to remove the solvent, obtaining an oily product containing DMF. Afterwards, the product was further extracted with ethyl acetate and hexane (1:1) and brine; the solvent of the recovered organic phase was evaporated with the rotary evaporator. After that, the product was purified using a separatory column chromatography applying petroleum ether and dichloromethane (5:2) as eluents. After the removal of the solvent, the solid product was furtherly purified by washing with a solution of boiling methanol, then filtered and dried to afford **iI-OD-Br2** with a yield of 76 %.

^{1}H NMR (CDCl3, 500MHz): δ 0.86 (t, 12H); 1.24-1.40 (m, 64H); 1.88 (s broad, 2H); 3.62 (d, 4H, *J*=7.5 Hz); 6.90 (s, 2H); 7.16 (d, 2H, *J*=8.5 Hz); 9.07 (d, 2H, *J*=8.5 Hz)

^{13}C NMR (CDCl3, 500 MHz): δ 14.5; 23.0; 26.7; 29.6; 29.7; 29.9; 30.0, 30.3; 31.8; 32.2; 32.3;36.4; 45.1; 111.9; 120.8; 125.4; 127.0; 131.4; 133.0; 146.6; 168.5.

FTIR (KBr): ν (cm^{-1}): 599.7; 816.8; 849.0; 884.2; 1066.7; 1124.8; 1320.6; 1452.4; 1611.1; 1686.1; 3134.9.

Synthesis of (*E*)-5,5'-(1,1'-bis(2-octyldodecyl)-2,2'-dioxo-[3,3'-biindolinylidene]-6,6'-diyl)bis(thiophene-2-carbaldehyde) (iI-T-CHO)

1.0g (1.03 mmol) of **iI-OD-Br$_2$** and 636 mg (4.08 mmol) of 5-formyl-2-thyenilboronic acid were dissolved in 20 mL of THF and placed in an inert atmosphere. The system was degassed by blowing nitrogen into the reaction flask with a needle. Then 2.2 ml of K_3PO_4 1.4 M in water were added. Finally, 24 mg (1.02 mmol) of $Pd_2(dba)_3$ and 14 mg (0.5 mmol) of $P(t\text{-}Bu)_3xHBF_4$ were added to the reaction system. The system was kept at reflux overnight; then, the solvent was removed using the rotary evaporator and the crude product was extracted with dichloromethane and water (1:1). The product obtained was recrystallized from hot ethanol to yield **iI-T-CHO** (0.815 g, 64%) as a dark brown solid.

^{1}H NMR ($CDCl_3$, 500 MHz): δ 0.84 (m, 12H); 1.23-1.41 (m, 64H); 1.95 (s broad, 2H); 3.73 (d, 4H, *J*=7.5 Hz); 7.04 (s, 2H); 7.38 (d, 2H, *J*=8.5 Hz); 7.49 (d, 2H, *J*=4.0 Hz); 7.77 (d, 2H. *J*=4.0 Hz); 9.26 (d, 2H, *J*=8.0 Hz); 9.93 (s, 2H).

^{13}C NMR ($CDCl_3$, 400 MHz): δ 14.3; 22.9; 26.8; 29.5; 29.6; 29.8; 30.2; 31.9; 32.1; 36.6; 44.9; 105.7; 120.2; 122.8; 125.2; 130.8; 132.8; 136.7; 137.3; 143.4; 146.2; 153.4; 168.4; 182.9.

FTIR (KBr): ν (cm^{-1}): 818.3; 871.9; 1113.6; 1281.9; 1382.9; 1460.4; 1611.6; 1670.6; 1691.1; 2852.7.; 2923.3.

CHN Analysis: Found: C 75.62, H 9.18, N 2.68, S 5.85 %; molecular formula for $C_{66}H_{94}N_2O_4S_2$ requires: C 75.96, H 9.08, N 2.68, S 6.14 %.

MS (MALDI-TOF) m/z: found 1043.31 [$(M+H)^+$]. Calculated for $C_{66}H_{94}N_2O_4S_2$: 1042.67.

Synthesis of (*E*)-5,5'-(1,1'-bis(2-octyldodecyl)-2,2'-dioxo-[3,3'-biindolinylidene]-6,6'-diyl)bis(furan-2-carbaldehyde) (iI-F-CHO)

iI-F-CHO was synthesized using the same procedure as described for the synthesis of **iI-T-CHO** apart from the purification step that was realized by means of liquid chromatography run on silica gel using dichloromethane as eluent. The desired product was obtained with a yield of 53%.

^{1}H NMR ($CDCl_3$, 500MHz): δ 0.85 (m, 12H); 1.22-1.42 (m, 64H); 1.98 (broad, 2H); 3.74 (d, 4H, *J*=7.5 Hz); 6.94 (d, 2H, *J*=3.5 Hz); 7.21 (s, 2H); 7.36 (d, 2H, *J*=3.5 Hz); 7.46 (d, 2H, *J*=8.5 Hz); 9.26 (d, 2H, *J*=8.5 Hz); 9.72 (s, 2H).

^{13}C NMR (CD_2Cl_2, 500 MHz): δ 14.4; 23.2; 27.1; 29.9; 30.1; 30.2; 30.3; 30.6; 32.2; 32.4; 32.5; 45.1; 104.6; 110.0; 119.2; 123.3; 130.9; 132.6; 133.1; 146.6; 153.1; 158.9; 168.6; 177.8.

FTIR (KBr): ν (cm^{-1}): 771.0; 793.0; 870.6; 1115.5; 1355.1; 1378.7; 1470.0; 1519.9; 1612.5; 1677.9; 1697.9; 2851.3.; 2920.9.

CHN Analysis: Found: C 78.12, H 9.47, N 2.66 %; molecular formula for $C_{66}H_{94}N_2O_6$ requires: C 78.37, H 9.37, N 2.77 %.

MS (MALDI-TOF) m/z: found 1011.34 [$(M+H)^+$]. Calculated for $C_{66}H_{94}N_2O_6$: 1010.71.

Synthesis of (*E*)-2,2'-((5,5'-(1,1'-diicosyl-2,2'-dioxo-[3,3'-biindolinylidene]-6,6'-diyl)bis(furan-5,2-diyl))bis(methanylylidene))dimalononitrile (iI-F-DCV)

300 mg (0.297 mmol) of iI-F-CHO, 78.6 mg (1.19 mmol) of malonitrile and 77 mg (0.864 mmol) of β-alanine were added to a round bottom flask with two necks and placed under nitrogen atmosphere. 24.0 mL of anhydrous 1,2-dichloroethane (DCE) and 6.0 mL of ethanol were added to the reaction system. The reaction was kept under stirring at reflux overnight. Then, the solvent was evaporated using a rotary evaporator; the solid residue was dissolved in the minimum amount of chloroform and precipitated in 100 ml of methanol. The solid was then recovered by suction filtration. Yield was 63%.

^{1}H NMR (CD_2Cl_2, 400MHz): δ 0.86 (d, 12H); 1.22-1.35 (m, 64H); 1.98 (s broad, 2H); 3.67 (d, 4H; *J*=7.6 Hz); 7.07 (d, 2H, *J*=3.6 Hz); 7.27(s, 2H); 7.29 (d, 2H, *J*=3.6 Hz); 7.41 (d, 2H, *J*=8 Hz); 7.44 (s, 2H); 9.26 (d, 2H, *J*=8.4 Hz).

^{13}C NMR ($CDCl_3$, 500MHz): δ 14.3; 22.9; 29.5; 29.6; 29.8; 29.9;30.3; 31.3; 32.1; 36.3; 45.1; 104.9; 111.3; 113.6; 114.4; 119.6; 123.6; 126.6; 130.8; 131.0; 132.9; 146.4; 147.9; 160.6; 168.1.

Melting point: 226 °C.

FTIR (KBr): ν (cm^{-1}): 792.8; 820.0; 870.2; 1031.7; 1142.3; 1329.7; 1369.9; 1441.2; 1465.0; 1541.1; 1600.7; 1697.9; 2244.5; 2852.0; 2922.6.

CHN Analysis: Found: C 77.89, H 8.63, N 7.39 %; molecular formula for $C_{72}H_{94}N_6O_4$ requires: C 78.08, H 8.55, N 7.59 %.

MS (MALDI-TOF) m/z: found 1107.42 [$(M+H)^+$]. Calculated for $C_{72}H_{94}N_6O_4$: 1106.73.

Synthesis of (*E*)-5,5'-((5,5'-(1,1'-diicosyl-2,2'-dioxo-[3,3'-biindolinylidene]-6,6'-diyl)bis(furan-5,2-diyl))bis(methanylylidene))bis(1,3-diethyl-2-thioxodihydropyrimidine-4,6(1H,5H)-dione) (iI-F-TB)

300 mg (0.297 mmol) of iI-F-CHO, 238 mg (1.19 mmol) of N,N-diethylthiobarbituric acid and 77 mg (0.864 mmol) of β-alanine were added to a round bottom flask with two necks and placed under nitrogen atmosphere. 24.0 mL of anhydrous 1,2-dichloroethane (DCE) and 6.0mL of ethanol were added to the reaction system. The reaction was kept under stirring at reflux overnight. Then, the solvent was evaporated using a rotary evaporator; the solid residue was dissolved in the minimum amount of chloroform and precipitated in 100 ml of methanol. The solid was then recovered by suction filtration. The yield was 67%.

^{1}H NMR ($CDCl_3$, 500MHz): δ 0.85 (d, 12H); 1.23-1.41 (m, 64H); 1.99 (s broad, 2H); 3.76 (d, 4H, *J*=7.5 Hz); 4.58 (q, 8H, *J*=6.0 Hz) 7.11 (d, 2H,*J*=4.0 Hz); 7.17 (s, 2H); 7.45(d, 2H, *J*=8.5 Hz) 8.43 (s, 2H); 8.83 (d, 2H, *J*=4.0 Hz); 9.27 (d, 2H, *J*=8.5 Hz).

^{13}C NMR ($CDCl_3$, 500MHz): δ 12.6; 12.7; 14.3; 22.9; 26.7; 29.6; 29.8; 29.9; 30.3; 31.8; 32.1; 36.5; 43.6; 44.3; 45.0; 104.2; 112.0; 113.2; 119.8; 123.6; 130.9; 131.5; 132.8; 140.0; 146.2; 152.0; 158.9; 160.9; 161.4; 168.3; 178.7.

Melting point: 266 °C.

FTIR (KBr): ν (cm^{-1}): 783.9; 815.2; 1040.8; 1116.1; 1286.5; 1389.0; 1550.4; 1573.8; 1661.1; 1690.9; 2852.8; 2923.8.

CHN Analysis: Found: C 71.24, H 8.60, N 5.94, S 4.58 %; molecular formula for $C_{82}H_{114}N_6O_8S_2$ requires: C 71.58, H 8.35, N 6.11, S 4.66 %.

MS (MALDI-TOF) m/z: found 1375.42 [$(M+H)^+$]. Calculated for $C_{82}H_{114}N_6O_8S_2$: 1374.81.

Synthesis of (*E*)-2,2'-((5,5'-(1,1'-diicosyl-2,2'-dioxo-[3,3'-biindolinylidene]-6,6'-diyl)bis(furan-5,2-diyl))bis(methanylylidene))bis(1H-indene-1,3(2H)-dione) (iI-F-ID)

300 mg (0.297 mmol) of **iI-F-CHO**, 174 mg (1.19 mmol) of 1,3-indandione and 77 mg (0.864 mmol) of β-alanine were added to a round bottom flask with two necks and placed under nitrogen atmosphere. 24.0 mL of anhydrous 1,2-dichloroethane (DCE) and 6.0 mL of ethanol were added to the reaction system. The reaction was kept under stirring at reflux overnight. Then, the solvent was evaporated using a rotary evaporator; the solid residue was dissolved in the minimum amount of chloroform and precipitated in 100 ml of methanol. The solid was then recovered by suction filtration. The yield was 72 %.

^{1}H NMR ($CDCl_3$, 500MHz): δ 0.82 (m, 12H); 1.21-1.42 (m, 64H); 1.99 (s broad, 2H); 3.76 (d, 4H, *J*=7.6 Hz); 6.96 (d, 2H, *J*=3.6 Hz); 7.07 (s, 2H); 7.31 (dd, 2H, *J*1= 8.4 Hz, *J*2=1.6 Hz); 7.52 (s, 2H); 7.65-7.67(m, 4H); 7.83-7.90 (m, 4H); 8.44 (s, 2H); 9.19 (d, 2H, *J*=8.4 Hz).

^{13}C NMR ($CDCl_3$, 500MHz): δ 14.3; 22.9; 26.6; 29.6; 29.8; 29.9; 30.2; 30.3; 31.7; 32.1; 36.5; 44.9; 104.1; 112.3; 119.1; 122.9; 123.0; 123.1; 124.1; 127.7; 130.7; 131.7; 132.4; 134.8; 135.1; 140.4; 142.5; 145.6; 151.7; 159.6; 168.3; 188.7; 190.0.

Melting point: 248 °C.

FTIR (KBr): ν (cm^{-1}): 733.7; 811.3; 870.5; 1193.3; 1350.9; 1471.1; 1514.1; 1578.7; 1678.1; 2851.9; 2922.6.

CHN Analysis: Found: C 79.16, H 8.28, N 2.20 %; molecular formula for $C_{84}H_{102}N_2O_8$ requires: C 79.58, H 8.11, N 2.21 %.

MS (MALDI-TOF) m/z: found 1267.38 [$(M+H)^+$]. Calculated for $C_{84}H_{102}N_2O_8$: 1266.76.

Synthesis of 2,2'-((2Z,2'Z)-((5,5'-((*E*)-1,1'-diicosyl-2,2'-dioxo-[3,3'-biindolinylidene]-6,6'-diyl)bis(furan-5,2-diyl)) bis(methanylylidene))bis(3-oxo-2,3-dihydro-1H-indene-2,1-diylidene))dimalononitrile (iI-F-IDM)

300 mg (0.297 mmol) of **iI- F-CHO**, 231 mg (1.19 mmol) of dicyanomethylene-3-Indanone and 77 mg (0.864 mmol) of β-alanine were added to a round bottom flask with two necks and placed under nitrogen atmosphere. 24.0 mL of anhydrous 1,2-dichloroethane (DCE) and 6.0 mL of ethanol were added to the reaction system. The reaction was kept under stirring at reflux overnight. Then, the solvent was evaporated using a rotary evaporator; the solid residue was dissolved in the

minimum amount of chloroform and precipitated in 100 ml of methanol. The solid was then recovered by suction filtration. The yield was 60 %.

^{1}H NMR ($CDCl_3$, 400MHz): δ 0.84 (m, 12H); 1.21-11.40 (m, 64H); 1.98 (s, 2H); 3.78 (d, 4H, *J*=7.2 Hz); 7.12 (d, 2H, *J*=4.0 Hz); 7.21 (s, 2H); 7.44 (d, 2H, *J*=8.4 Hz); 709-7.48 (m, 4H); 7.87 (d, 2H, *J*=6.8 Hz); 8.51 (s, 2H); 8.66 (m, 4H); 9.27 (d, 2H, *J*=8.4 Hz).

^{13}C NMR ($CDCl_3$, 500MHz): δ 14.3; 22.9; 29.6; 29.8; 29.9; 30.0; 30.3; 31.7; 32.1; 36.6; 44.9; 70.7; 104.1; 113.4; 114.6; 119.5; 123.5; 123.8; 123.9; 125.3; 128.2; 130.6; 130.9; 131.0; 132.4; 132.5; 135.2; 137.2; 139.8; 146.0; 151.2; 159.9; 161.0; 138.0; 186.9.

Melting point: 238 °C.

FTIR (KBr): ν (cm^{-1}): 722.0; 802.1; 871.0; 1116.2; 1240.6; 1342.5; 1458.9; 1504.7; 1560.9; 1594.3; 1701.5; 2851.9; 2923.5.

CHN Analysis: Found: C 79.05, H 7.72, N 5.99 %; molecular formula for $C_{90}H_{102}N_6O_6$ requires: C 79.26, H 7.54, N 6.16 %.

MS (MALDI-TOF) m/z: found 1363.37 [$(M+H)^+$]. Calculated for $C_{90}H_{102}N_6O_6$: 1362.79.

Synthesis of (*E*)-2,2'-((5,5'-(1,1'-diicosyl-2,2'-dioxo-[3,3'-biindolinylidene]-6,6'-diyl)bis(thiophene-5,2-diyl))bis(methanylylidene))dimalononitrile (iI-T-DCV)

300 mg (0.287 mmol) of **iI-T-CHO**, 76.0 mg (1.15 mmol) of malononitrile and 77 mg (0.864 mmol) of β-alanine were added to a round bottom flask with two necks and placed under nitrogen

atmosphere. 24.0 mL of anhydrous 1,2-dichloroethane (DCE) and 6.00 mL of ethanol were added to the reaction system. The reaction was kept under stirring at reflux overnight. Then, the solvent was evaporated using a rotary evaporator; the solid residue was dissolved in the minimum amount of chloroform and precipitated in 100 ml of methanol. The solid was then recovered by suction filtration. The yield was 57 %.

^{1}H NMR ($CDCl_3$, 500MHz): δ 0.84 (m, 12H); 1.20-1.38 (m, 64H); 1.90 (s broad, 2H); 3.71 (d, 4H, *J*=8.5 Hz); 6.98 (d, 2H, *J*=1.5 Hz); 7.35 (dd, 2H, *J*1=8.5 Hz, *J*2==1.5 Hz); 7.49 (d, 2H, *J*=4.5 Hz); 7.76 (d, 2H, *J*=4.5 Hz); 7.77 (s, 2H); 9.24 (d, 2H, *J*=8.5 Hz)

^{13}C NMR ($CDCl_3$, 500MHz): δ 14.3; 22.9; 26.8; 29.5; 29.6; 29.8; 29.9; 30.2; 31.9; 32.1; 36.7; 44.9; 105.7; 113.3; 114.1; 120.6; 123.5; 125.9; 131.0; 133.0; 135.3; 135.8; 139.6; 146.4; 150.3; 155.3; 168.3.

Melting point: 248 °C.

FTIR (KBr): ν (cm^{-1}): 805.4; 872.6; 1073.8; 1113.9; 1261.3; 1327.3; 1428.0; 1567.6; 1610.1; 1694.8; 2220.8; 2852.8; 2923.7.

CHN Analysis: Found: C 75.62, H 8.65, N 7.11, S 5.82 %; molecular formula for $C_{72}H_{94}N_6O_2S_2$ requires: C 75.88, H 8.31, N 7.37, S 5.63 %.

MS (MALDI-TOF) m/z: found 1139.32 [$(M+H)^+$]. Calculated for $C_{72}H_{94}N_6O_6S_2$: 1138.69.

Synthesis of (*E*)-5,5'-((5,5'-(1,1'-diicosyl-2,2'-dioxo-[3,3'-biindolinylidene]-6,6'-diyl)bis(thiophene-5,2-diyl))bis(methanylylidene))bis(1,3-diethyl-2-thioxodihydropyrimidine-4,6(1H,5H)-dione) (iI- T-TB)

300 mg (0.287 mmol) of **iI-T-CHO**, 230 mg (1.15 mmol) of 1,3-diethyl-2-thiobarbituric acid and 77 mg (0.864 mmol) of β-alanine were added to a round bottom flask with two necks and placed under nitrogen atmosphere. 24.0 mL of anhydrous DCE and 6.0 mL of ethanol were added to the reaction system. The reaction was kept under stirring at reflux overnight. The reaction mixture was cooled at room temperature and the precipitation of a solid occurred. The precipitate was recovered by suction filtration and washed in 100 ml of methanol. A violet solid was recovered by suction filtration. Yield was 65 %.

^{1}H NMR ($CDCl_3$, 500MHz): δ 0.86 (m, 12H); 1.22-1.39 (m, 64H); 1.98 (s broad, 2H); 3.78 (d, 4H, *J*=7.5 Hz); 4.63 (q, 8H, *J*=7.0 Hz) 7.14 (s, 2H); 7.51 (dd, 2H, *J*1=7.5 Hz, *J*2=4.0 Hz); 7.60 (d, 2H, *J*=4.5 Hz); 7.92 (d, 2H, *J*=4.5 Hz); 8.69 (s, 2H); 9.28 (d, 2H, *J*=8.0 Hz).

^{13}C NMR ($CDCl_3$, 500MHz): δ 12.6; 12.7; 14.3; 22.9; 26.8; 29.6; 29.8; 29.9; 30.2; 31.9; 32.1; 43.4; 44.2; 44.8; 105.8; 111.2; 120.9; 123.4; 125.8; 130.9; 132.9; 136.8; 137.9; 146.3; 146.9; 149.4; 160.0; 161.1; 168.4; 178.9.

Melting point: 212 °C

FTIR (KBr): ν (cm^{-1}): 800.7; 873.4; 1103.2; 1262.4; 1343.3; 1397.5; 1548.8; 1658.8; 1698.3; 2852.8; 2922.5.

CHN Analysis: Found: C 70.09, H 7.90, N 5.92, S 8.85 %; molecular formula for $C_{82}H_{114}N_6O_6S_4$ requires: C 69.94, H 8.16, N 5.97, S 9.11 %.

MS (MALDI-TOF) m/z: found 1407.30 [$(M+H)^+$]. Calculated for $C_{82}H_{114}N_6O_6S_4$: 1406.77.

Synthesis of (*E*)-2,2'-((5,5'-(1,1'-diicosyl-2,2'-dioxo-[3,3'-biindolinylidene]-6,6'-diyl)bis(thiophene-5,2-diyl))bis(methanylylidene))bis(1H-indene-1,3(2H)-dione) (iI-T-ID)

300 mg (0.287 mmol) of **iI-T-CHO**, 168 mg (1.15 mmol) of 1,3-indandione and 77 mg (0.864 mmol) of β-alanine were added to a round bottom flask with two necks and placed under nitrogen atmosphere. 24.0 mL of anhydrous DCE and 6.0 mL of ethanol were added to the reaction system. The reaction was kept under stirring at reflux overnight. The reaction mixture was cooled at room temperature and the precipitation of a solid occurred. The precipitate was recovered by suction filtration and washed in 100 ml of methanol. A green solid was recovered by suction filtration. Yield was 55 %.

1H NMR ($CDCl_3$, 500MHz): δ 0.83 (m, 12H); 1.21-1.39 (m, 64H); 1.97 (s broad, 2H); 3.76 (d, 4H, *J*=7.0 Hz); 7.07 (s, 2H) 7.43 (dd, 2H, *J*1=8.5 Hz, *J*2=1.5 Hz); 7.51 (d, 2H, *J*=4.0 Hz); 7.78-7.79 (m, 4H) 7.92 (s, 2H); 7.96-7.99 (m, 4H); 8.03 (d, 2H, *J*=4.= Hz); 9.24 (d, 2H, *J*=8.0 Hz).

^{13}C NMR ($CDCl_3$, 500MHz): δ 14.3; 22.9; 26.9; 29.6; 29.8; 29.9; 30.3; 32.0; 32.1; 36.7; 44.8; 105.7; 120.5; 123.0; 123.1; 123.3; 125.0; 126.0; 130.8; 131.7; 135.1; 135.8; 136.9; 137.9; 140.7; 142.3; 143.2; 146.2; 156.1; 168.5; 189.6; 190.4.

Melting point: 301 °C

FTIR (KBr): ν (cm^{-1}): 799.9; 871.6; 1114.8; 1217.6; 1347.3; 1373.3; 1575.3; 1597.0; 1677.1; 2852.5; 2924.8.

CHN Analysis: Found: C 77.35, H 8.02, N 1.95, S 4.92 %; molecular formula for $C_{84}H_{102}N_2O_6S_2$ requires: C 77.62, H 7.91, N 2.16, S 4.93 %.

MS (MALDI-TOF) m/z: found 1299.27 [$(M+H)^+$]. Calculated for $C_{84}H_{102}N_2O_6S_2$: 1298.72.

Synthesis of 2,2'-((2Z,2'Z)-((5,5'-((*E*)-1,1'-diicosyl-2,2'-dioxo-[3,3'-biindolinylidene]-6,6'-diyl)bis(thiophene-5,2-diyl))bis(methanylylidene))bis(3-oxo-2,3-dihydro-1H-indene-2,1-diylidene))dimalononitrile (iI-T-IDM)

300 mg (0.287 mmol) of iI-OD-T-CHO, 223 mg (1.15 mmol) of 1,1-Dicyanomethylene-3-Indanone and 77 mg (0.864 mmol) of β-alanine were added to a round bottom flask with two necks and placed under nitrogen atmosphere. 24.0 mL of anhydrous DCE and 6.0 mL of ethanol were added to the reaction system. The reaction was kept under stirring at reflux overnight. The reaction mixture was cooled at room temperature and the precipitation of a solid occurred. The precipitate was recovered by suction filtration and washed in 100 ml of methanol. A deep blue solid was recovered by suction filtration. Yield was 65%.

^{1}H NMR ($CDCl_3$, 500MHz): δ 0.83 (m, 12H); 1.20-1.41 (m, 64H); 1.97 (s broad, 2H); 3.77 (s, 4H); 7.14 (s, 2H) 7.49 (d, 2H, *J*=8.5 Hz); 7.56 (d, 2H, *J*=4.0 Hz); 7.78 (m, 4H); 7.90 (d, 2H, *J*=4.0 Hz); 7.96 (d, 2H, *J*= 8.5 Hz); 8.72 (d, 2H, *J*=8.5 Hz); 8.88 (s, 2H); 9.27 (d, 2H, *J*=8.5 Hz).

^{13}C NMR ($CDCl_3$, 600MHz, 60°C): δ 14.0; 22.6; 26.7; 29.3; 29.5; 29.6; 30.1; 31.9; 32.1; 36.6; 44.9; 70.8; 105.5; 120.5; 124.0; 125.5; 125.6; 130.9; 132.7; 134.6; 135.3; 136.6; 137.2; 137.4; 137.5; 140.2; 145.2; 146.3; 156.1; 160.2; 168.3; 187.8.

Melting point: 277 °C

FTIR (KBr): ν (cm^{-1}): 797.3; 873.1; 990.5; 1111.5; 1222.0; 1326.4; 1396.3; 1548.3; 1567.1; 1604.9; 1697.9; 2851.2; 2920.7.

CHN Analysis: Found: C 77.70, H 7.46, N 5.86, S 4.62 %; molecular formula for $C_{90}H_{102}N_6O_4S_2$ requires: C 77.44 H 7.37, N 6.02, S 4.59 %.

MS (MALDI-TOF) m/z: found 1395.26 [$(M+H)^+$]. Calculated for $C_{90}H_{102}N_6O_4S_2$: 1394.74.

2.3. Computational analysis

The ground-state electronic structure of the dyes was calculated with density functional theory (DFT) methods, whereas the excited states and the absorption spectra were simulated with linear-response time dependent DFT (LR-TDDFT) calculations. Hybrid functionals of varied types, differing by the Hartree–Fock exchange percentage, were employed in the initial phase, in order to evaluate the best performing method in the calculation of HOMO-LUMO transition wavelength values among all the dyes investigated, assessed through the calculation of the average difference between calculated and experimental figures (see Tables S2-3). It is important to stress at this stage that the choice of other benchmarks (e. g. the ground-state HOMO energy obtained from cyclic voltammetry, see above) may lead to different scores. The following Density Functionals were tested: CAM-B3LYP, [28] PBE0 [29] and M06-2X;[30] the polarized 6–31+G(d,p) basis set was used in all the calculations, and the solvent effect of chloroform (static dielectric permittivity ε=4.711300, dielectric permittivity at infinite frequency ε(∞)=2.090627) was taken into account by using the Polarizable Continuum Model (PCM) formalism (IEF variant,[31]) as implemented in the code Gaussian.[32] PBE0 and M06 functionals gave the best results, with the former scoring an average HOMO/LUMO transition wavelength deviation of +66.86 nm (redshifted), while the latter scored -67.39 nm (blueshifted). The commonly used CAM-B3LYP functional behaved worse (-78.40). Very surprisingly, the use of the simpler basis-set 6-31G(d) without diffuse functions and hydrogen polarization gave the best result among all the method tested (average +55.11) whereas other functionals with 6-31+G(d) resulted in much poorer scores in the calculations of PF1

transitions only (blueshifted: W-B97XD (-77.52); LC-wHPBE (-143.80) – redshifted: B3LYP (+107.99); HSEH1PBE (109.39)) as use of PBE0 with larger basis-sets (6-311++g(d,p) (71.23); aug-CCPVTZ (84.08). Apparently anomalous trends like this have already been described with PCM calculations of spectroscopic properties in the past, the reason for error cancellations being not always straightforward to be identified. [33] The final choice was therefore PBE0/6-31G(d), owing to the good reproduction of UV-Vis absorption patterns (average peak positions within 0.17 eV). The long 8- and 10-membered alkyl chains were replaced by methyl groups for simplicity and the geometries of the molecules were optimized in a three-stage process, made up of a first Hartree-Fock relaxation with the same basis set using standard minimization techniques, [34] followed by the DFT/PCM optimization and finally by the LR-time-dependent excitation analysis (vertical transitions) on the optimized geometry. The obtained conformation (*vide infra*) should be regarded as a "near" local minimum on the potential energy surface (PES), that was not investigated completely, given its complexity. Yet, sample tests on other conformations were run, e. g. the "cis" arrangement of furan and tiophene moieties led to slightly higher energies and to similar UV-Vis patterns). To verify that the stationary points found were real minima on the PES, the calculation of the vibrational frequencies was carried out, and no imaginary values were found in any case.

All QM computations were performed with G16 package, whereas the analysis of the percentage contributions to the calculated TD-DFT spectra was accomplished with the code GaussSum 3.0 [35] and the spectra were built with the code Gaussview, [36] by assigning to each vertical transition (line) a Gaussian function with Half-Width at Half Height (HWHH) equal to 0.15 eV (1209.83 cm^{-1}).

2.4 ***Electrical characterization***

Solutions of the investigated compounds were prepared in $CHCl_3$/TCE 95/5 % v/v solution at a 5 mg/ml concentration. The solutions were then spin-coated on the substrates (see below) at 1000 rpm for 1 minute and then at 2000 rpm for 30 s. After the deposition, films were annealed in a vacuum oven, at 120 °C, for 1 h. The resulting final thicknesses were comprised in the range between 15 and 30 nm.

In this study, bottom-gate bottom-contact field-effect transistors were achieved by using multilayer structures including a 500-µm thick highly-doped silicon (Si^{++}), working as substrate and gate electrode, a 200-nm thick SiO_2 dielectric barrier and 150-nm thick pre-patterned source/drain interdigitated gold electrodes. Before the film deposition, the SiO_2 surface was carefully functionalized by applying HMDS (hexamethyldisilazane) self-assembling monolayers in order to increase the SiO_2 surface water-contact angle (θ_C) up to ~110° and to attenuate the possible impact of charge trapping phenomena ascribable to the physisorption of water molecules on the dielectric surface.[37]

The final devices were characterized by active channels featuring lengths of 20 or 40 µm and width/length (W/L) ratios of 550. In the last years, this configuration was successfully employed to characterize both semiconducting (mobility down to 10^{-7} $cm^2/V\cdot$) and semi-insulating (conductivity down to 10^{-8} S/cm) organic compounds.[38] For all the electrical measurements here discussed, the field-effect transistors were mounted in a Janis cryogenic probe station and tested in vacuum (base pressure P_r ~ 10^{-5} mbar) by a Keithley 4200 Semiconductor Parameter Analyzer in such a way to contemporarily apply the gate-source (V_{GS}) and drain-source (V_{DS}) voltages while measuring the related I_{DS} and I_{GS} currents. Both transfer- (I_{DS} vs V_{GS} at fixed V_{DS}) and output (I_{DS} vs V_{DS} at fixed V_{GS}) curves were recorded for the electrical characterization.

Field-effect electron mobility (µ) and threshold voltage (V_{th}) values were extracted from the transfer-curves measured in the saturation regime (V_{DS}= + 50V) by using the MOSFET equation to fit linearly the square root of the experimental curve:

$$\sqrt{I_{ds}} = \sqrt{\frac{W}{2L} C_{ox} \mu^{*}} (V_{GS} - V_{th}) \qquad (1)$$

with C_{ox} (i.e., the oxide capacitance per unit area) being here equal to 17.25 nF/cm^2.

3. Results and discussion

3.1. Synthesis

The dyes were prepared through a synthetic procedure consisting of four steps, highlighted in Scheme 3. **iI** unit was prepared in a nearly quantitative yield by the condensation of 6-bromoisatin with 6-bromooxindole, in glacial acetic acid and with a catalytic amount of HCl, as reported in the literature.[27] Then, by reaction with 2-octyldodecyl-bromide in DMF under basic conditions (K_2CO_3), **iI** was N-alkylated (**iI-OD**) to achieve the desired solubility. Subsequently, this brominated derivative was reacted in a Suzuki-Miyaura cross-coupling reaction to extend the molecular backbone. In a first attempt, the reaction was performed with $Pd(PPh_3)_4$ used as catalyst but with poor yields and a demanding workup. Following a recent literature procedure,[39] a different catalytic system consisting of $Pd(dba)_3$ as a catalyst and $P(t\text{-}bu)_3xHBF_3$ as a co-catalyst, was used; this catalytic system was dissolved with 5-formyl-2-thiophenboronic acid (for T-series) or 5-formyl-2-furanboronic acid (in F-series), in THF while K_3PO_4 was used as base. The desired di-formyl derivatives **iI-F-CHO** and **iI-T-CHO** were obtained in good yields. In the last reaction step, different auxiliary electron-accepting groups were introduced through a Knoevenagel reaction. The aldehydic groups of the common precursors reacted in a basic environment with compounds containing acid methylene groups (malononitrile, N,N-diethylthiobarbituric acid and two indandione derivatives) to obtain the desired dyes with yields up to 76 %.

The chemical identity of the synthesized dyes was confirmed by elemental analysis, mass spectroscopy and NMR analysis. In ^{1}H-NMR analysis a particularly significant resonance is that associated to the proton of the methine bridge connecting the central part of the molecules to the end acceptor groups: this singlet is shifted at higher chemical shift values as the strength of the EWGs increases. Indeed, regarding the T-series (Figures S2-S5), the methine signal resonates at

8.88 ppm in the case of the dye functionalized with the strongest EWG, **iI-OD-T-IDM**, 8.69 ppm in the case of **iI-OD-T-TB**, 7.92 ppm in the case of **iI-OD-T-ID**, and 7.77 ppm in the case of **iI-OD-T-DCV**, which is the weakest EWG. The same trend is observed for F-series (Figures S7-S10), where the methine signal resonates at 8.51 ppm in the case of the dye functionalized with the strongest EWG, **iI-OD-F-IDM**, 8.43 ppm in the case of **iI-OD-F-TB**, 7.52 ppm in the case of **iI-OD-F-ID**, and 7.27 ppm in the case of **iI-OD-F-DCV**, which is the weakest EWG. ^{1}H-NMR of the T-series and F-series dyes exhibits similar patterns with chemical shifts moving to slightly lower δ values for the F-series.

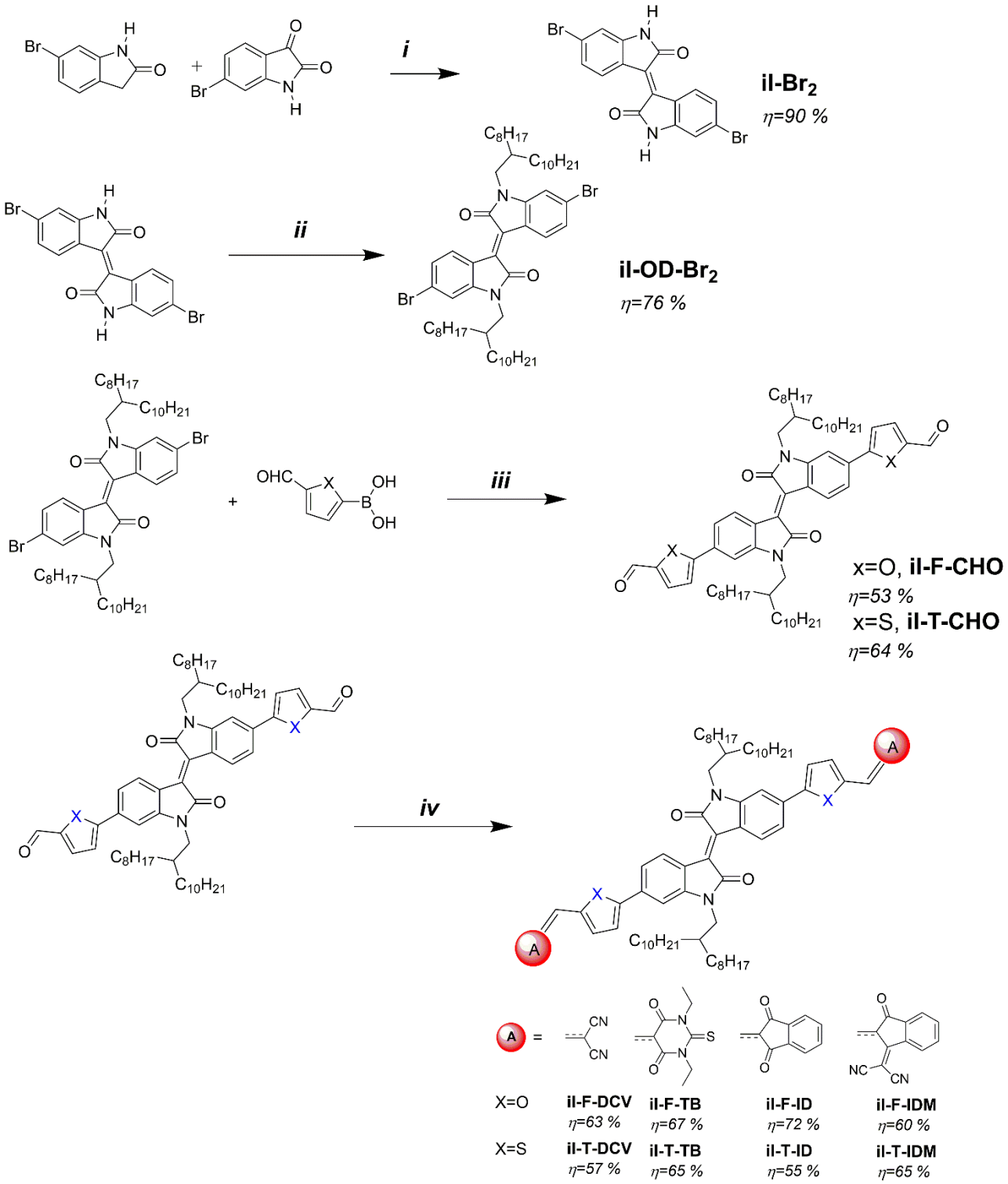

Scheme 3. Synthetic procedure followed for the preparation of the dyes; i) in CH_3COOH/conc. HCl(*cat.*), reflux, 20 h; ii) K_2CO3, 1.5 eq. of 1-bromo-2-octyldodecane, DMF, 110°C, run in N2, 20 h; iii) 2 eq. of 5-formyl-2-furanylboronic acid or 5-formyl-2-thienylboronic acid, $Pd_2(dba)_3$, $P(t\text{-}Bu)_3$ x

HBF_4, dry THF, N_2, reflux, 20 h; iv) 2 eq. of acceptor, dichloroethane-ethanol 4:1, β-alanine, reflux, 20 h, run in N_2.

3.2. Thermal analysis

Melting points of the synthesized dyes were determined by means of DSC analysis (see Figures S21-28) and are reported in Table 1. Moreover, the thermal stability of the new molecules was assessed by a thermogravimetric analysis (TGA) conducted at 20 °C/min in air. The decomposition temperature (T_d) was defined as the temperature at which the sample loses 5% of its starting mass. TGA thermograms are shown in Figure 1 while T_d values are reported in Table 1. All the dyes feature high thermal stability: all of them have in fact decomposition temperatures in air exceeding 360 °C with **iI-T-DCV** and **iI-F-DCV's** T_d values approaching 400°C.

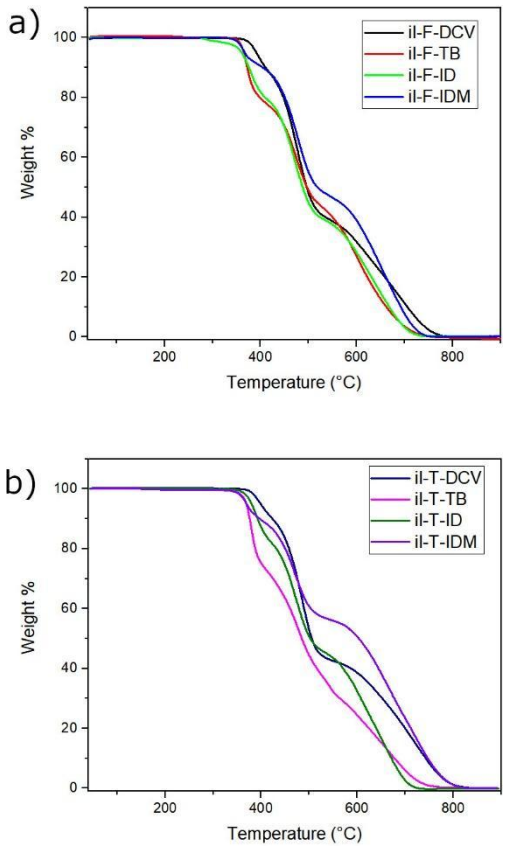

Figure 1. TGA analysis of the dyes performed in air; a) F-Series, b) T-Series.

Table 1. Thermal properties of the prepared compounds and optical properties of the dyes in $CHCl_3$ solution

Dyes	T_m (°C)[a]	T_d(°C)[b]	λ_1(nm)/$\varepsilon_{\lambda1}$($cm^{-1}\cdot M^{-1}$)[c]	λ_2(nm)/$\varepsilon_{\lambda2}$($cm^{-1}\cdot M^{-1}$)[c]
iI-F-DCV	226	394	458/$4.4\cdot10^4$	584/$3.6\cdot10^4$
iI-F-TB	266	365	482/$7.3\cdot10^4$	609/$7.7\cdot10^4$
iI-F-ID	312	360	471/$5.8\cdot10^4$	603/$5.7\cdot10^4$
iI-F-IDM	238	366	523/$3.5\cdot10^4$	637/$5.1\cdot10^4$
iI-T-DCV	248	397	452/$5.1\cdot10^4$	569/$3.2\cdot10^4$
iI-T-TB	213	370	484/$4.9\cdot10^4$	567/$5.5\cdot10^4$
iI-T-ID	301	378	471/$5.8\cdot10^4$	587/$4.6\cdot10^4$
iI-T-IDM	277	368	511/$5.9\cdot10^4$	616/$8.3\cdot10^4$

a) Melting temperatures determined by DSC analysis run at 10 °C/min in nitrogen atmosphere; b) decomposition temperature determined as the temperature corresponding to a weight loss of 5 % in a thermogravimetric experiment run in air at 10°C/min; c) absorption maxima and corresponding molar extinction coefficient in chloroform solution.

3.3. Optical properties in chloroform solutions

The optical properties of the synthesized dyes were investigated by UV-Vis absorption spectroscopy, performed both in chloroform solution. In Figure 2 the UV-Vis absorption spectra recorded in chloroform solution are presented.

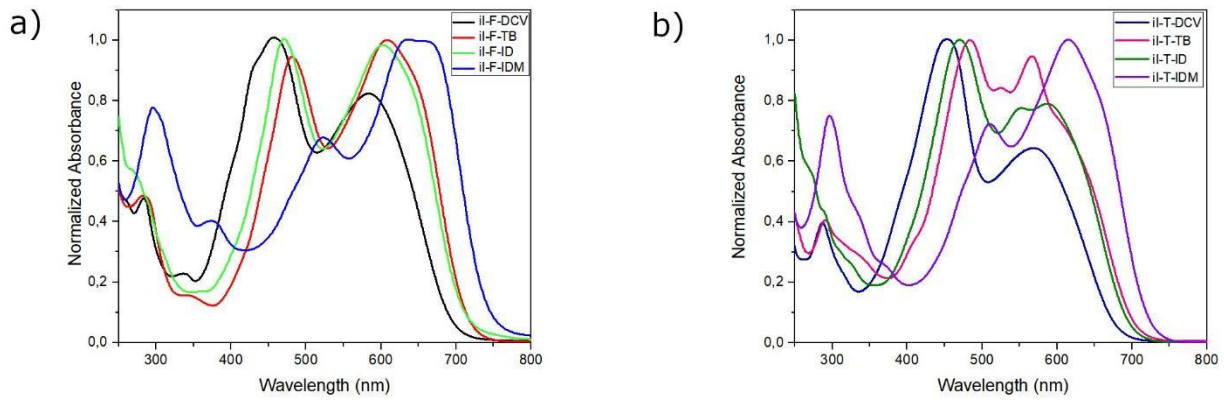

Figure 2. Optical spectra of the synthesized dyes in chloroform solution.

Qualitatively, optical spectra for the dyes of both series are characterized by multiple peaks with two main absorption features in the visible: the first one, at higher energy, occurs in the blue-green zone of the spectrum, while the second, ascribable to an ICT transition, occurs at wavelengths approaching or surpassing 600 nm. Both these optical features are influenced by the strength of the terminal EWGs so that along the increase of this strength, the wavelengths of absorption maxima experienced a red shift, as shown in Table 1. For what concerns **il-T-TB**, the lower energy absorption peak occurs at 567 nm, hence at lower wavelength of **il-T-ID** (587 nm), characterized by a weaker EWG terminal group: actually, the presence of a clear shoulder at ~600 nm seems to confirm the proposed trend. By comparing the two different series of dyes, F-series absorption is slightly red-shifted as compared to T-series and this could be a consequence of the lower aromaticity of the furan ring as compared to thiophene. Quantitatively, all the dyes feature a fair good light harvesting ability, with molar extinction coefficients, reported in Table 1, ranging from ~$3 \cdot 10^4$ to ~$8 \cdot 10^4$ $cm^{-1} \cdot M^{-1}$. The dyes are not soluble in methanol and other polar solvents as DMSO or DMF. Beyond chloroform, the dyes show a good solubility in 1,1-2,2-tetrachloroethane and a lower solubility in solvents like xylene and THF. Optical spectra of the dyes' solution in xylene and

THF were recorded and shown in Figure S29-S30. Qualitatively, the spectra resemble those recorded in chloroform with generally a slight blue shift (see Table S1) of the absorption peaks.

3.4. Calculations on the opto-electronic properties of the dyes

As described in the experimental section, several hybrid functionals were tested in the initial phase (see Tables S2-S3) and the choice fell on PBE0/6-31G(d) which was able to provide the best reproduction of the experimental UV-Vis absorption patterns and average peak positions, kept within 0.17 eV. The DFT-PCM geometry optimizations, that was performed without imposing any structural constraint, led to quite symmetrical structures in all the eight dyes. Indeed, the final geometries of the molecules, disregarding the alkyl chains (here modelled as a methyl group) can be described as S-shaped arrangements with a central **iI** core. The optimized configurations belong to C_2 point group symmetry with a high degree of confidence, neglecting the small numerical deviations. Yet, though such highly symmetrical arrangement is meaningful only in *in vacuo* calculations, still it is a useful aid for the interpretation. The molecule can be divided into three fragments (see Figure 3 and Table 2), connected by the three torsion angles D1, D2, D3 around, respectively, the bond linking the external fragments with furan/tiophene ring, the bond between furan/tiophene and **iI** core and the link between the two oxindole portions of **iI**. The dihedral angles D1 and D2 appear twice (D1' and D2') and have very similar values owing to the aforementioned symmetry. The following structural features can be pointed out: the central **iI** torsion (D3) falls in the range 13-14.5 degrees (absolute value) and has negative sign apart from the two dyes bearing **TB** as outer fragment. Outer fragments and furan/tiophene are almost coplanar (small dihedral angles D1, ranging from -1.5 to 1.5 degrees), whereas the connection between **iI** and furan/tiophene moieties has quite different angles for the two eteroaromatics: furan is almost coplanar with isoindigo, while in T-series dyes, because of the bigger size of sulfur (as compared to oxygen) dihedral angle D2 ranging from -22 to -24 degrees is observed. Depending

on the relative sign of D2 and D3 and on their summation, the overall geometry of the molecule may have larger or smaller curvature, as it appears, for instance, in **iI-T-TB** (negative D2/D2' and positive D3/D3'), whose conformation is wavy. The angular values are reported in Table 2, and the cartesian coordinates of each compound are included as additional material.

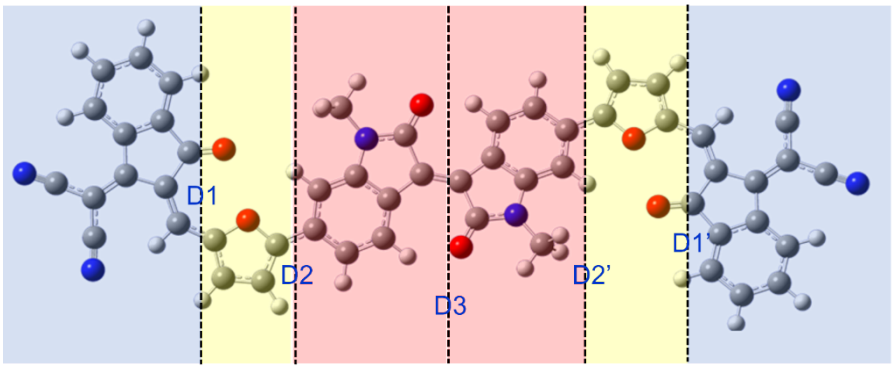

Figure 3. Schematic representation of the dyes' torsional patterns

Table 2: Calculated dihedral angles (as defined in Figure 3) in the optimized geometry of the dyes.

Dyes	D1	D2	D3
iI-F-DCV	-0.07	-0.61	-14.41
iI-F-TB	-1.05	1.56	14.11
iI-F-ID	-0.11	0.25	-13.69
iI-F-IDM	1.29	0.84	-13.84
iI-T-DCV	0.01	-22.13	-13.32
iI-T-TB	1.45	-23.61	13.59
iI-T-ID	0.04	-20.76	-13.43
iI-T-IDM	0.22	-22.66	-13.41

The theoretical spectra built from the fifty-excitation transitions explored by TDDFT procedure are reported in Fig. 4 and appear in satisfactory agreement with the experimental ones reported in Fig. 2. They are made up of three intense peaks (four in **iI-F-DCV**) in the range 250-1000 nm and the agreement is not limited to the highest λ used for the functional choice, thus validating the overall procedure.

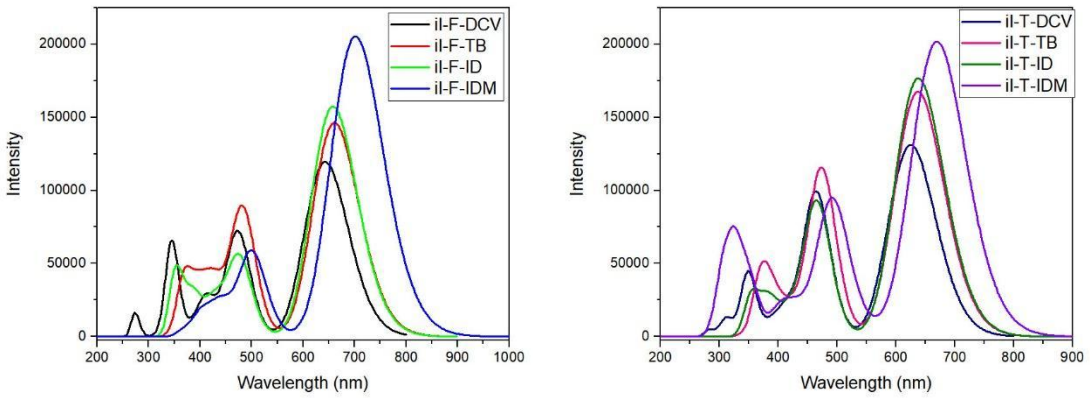

Figure 4. Theoretical UV-Vis spectra of the dyes. F-series: left panel; T-series: right panel

The general slight decrease in wavelength when passing from furan to tiophene dyes, observed in the experimental spectra, is respected; at the same time, the wavelength of absorption maxima becomes longer as the strength of terminal EWGs increases, thus confirming the experimentally observed trend. The corresponding transition wavelengths, energy, oscillator strengths (larger than 0.1) and percent contribution (larger than 10%) of a given transition between ground state orbitals to the excited state [40] are reported fully in Table S4-S5. The higher wavelength absorption bands, which correspond almost entirely to HOMO→LUMO transitions, are reported in Table 3, together with the dipole moments of ground and excited states, HOMOs and LUMOs energies, optical band gap calculated in the TD-DFT vertical transition (Optical E_g) and ground-state electronic band gaps (LUMO-HOMO difference).

As can be noticed in Table 3, all chromophores but **iI-T-IDM** show an increase in the overall dipole moment values when passing from ground to excited state, that is larger for **iI-T-DCV** and **iI-T-ID**. The peculiar dipole moment decrease upon excitation shown by **iI-T-IDM** was actually observed also in the previously reported **DPP** parent compound end-functionalized with **IDM** acceptor. [22] The most important components of the dipole moment vector lie on an axis approximately orthogonal to the average **iI** plane (Z-axis) whereas, given the C_2 symmetry of the molecule, the components along the X (longitudinal, i. e. directed along the molecular backbone direction) and Y-axis (transverse) are close to zero. For what concerns frontier's orbital energies, it is possible to observe that furan containing dyes (F-series) feature lower energy HOMOs as compared to thiophene analogues (T-series) while LUMO energies seem to be almost unaffected by the nature of the heterocycle. Focusing on the effect of the terminal acceptors, a difference is observed with respect to the **DPP** derivatives previously investigated:[22] those dyes differ from the here reported ones only for the central part, constituted by a dithienyl-diketopyrrolopyrrole rather than isoindigo. In the previous work, LUMO energies tended to be stabilized as the strength of the terminal EWGs (the same used here) increased; in the current work such trend is not confirmed. Indeed, we observed that while the most relevant stabilizing effect on dye's LUMO is still provided by the strongest EWG (**IDM**), **DCV** terminal acceptor group (the weakest EWG) shows an effect similar to that of **TB** (with **TB-DCV** order swapping between the two heteroaromatics) and higher than **ID**. The ranking of computed LUMO-HOMO energy differences among the dyes complies, qualitatively well with calculated TD-DFT transition energies and with experimental data, signalling that the excitonic effects are satisfactorily accounted for by the computational strategy chosen.

The charge density variations can be investigated, as well, by inspecting the total differential electron distribution maps between excited and ground states (difference electron densities) which are shown in Figure 5 for all the chromophores: magenta lobes correspond to positive

values of the difference ES – GS, i.e., larger values in the excited state, while green surfaces correspond to negative ones (electron depletion) in the excited state. From the analysis of the isosurfaces, it appears evident that the strongest EWG (**IDM**) is capable of attracting the charge density furthest away from the center: moving from the donor heterocycles to the terminal acceptors, electron density "travel" alongthree bonds in **iI-F/T-IDM** in compliance with a larger conjugation that results in the maximal effect on UV-Vis absorption wavelength lowering. A similar density increase (magenta lobes near the EWG group in the excited state) is seen for **DCV** terminal acceptor as well, but the travelled path is smaller. These finding, cannot be easily related to the variation of the dipole moment between GS and ES (since the latter occurs mainly along the orthogonal axis (i. e. above/below the central core). The dipole variation is relevant in both **iI-T-IDM** and **iI-T-DCV**, but it occurs with opposite signs (+0.45 and -0.34), featuring a negative value in **iI-T-IDM**. In the latter case, the system appears to undergo an extended charge density transfer from the center to the periphery (along x-axis) by looking at the density isosurfaces but a larger density transfer evidently occurs from above the plane towards the center of the isoindigo core to account for Δμ negative value. Smaller effects are seen in **TB** and **ID** functionalized dyes

difference densities where most of the variations occur in the area surrounding **iI** core. The analysis of HOMO and LUMO densities of the ground states, shown in Figures S31-S32, confirms that in the dyes bearing **DCV** and **IDM** acceptors, LUMOs present a larger sizeable orbital density accumulation around the dicyanovinyl substituent with respect to HOMOs: hence, upon the HOMO-LUMO transition, electron density moves from the **iI** core to the peripheral part of the molecules. In a lower extent, the same behaviour is shown by **TB** functionalized dyes and is the same also in the parent DPP derivatives previously reported. [22] In the case of **ID** terminated dyes, the opposite direction is observed with the electrons that move toward the **iI** core.

Table 3. Computed electronic and optical properties of the synthesized dyes

Dyes⟶	**IIl-F-DCV**	**IIl-F-TB**	**IIl-F-ID**	**IIl-F-IDM**	**IIl-T-DCV**	**IIl-T-TB**	**IIl-T-ID**	**IIl-T-IDM**
λ_{max}(nm)	642.92	660.98	658.11	701.82	625.38	637.67	638.16	677.13
f^{a}	1.33	1.63	1.75	2.28	1.46	1.86	1.97	2.48
H⟶L contrib. % [b]	97	97	97	96	97	96	97	95
μ_{GS}(D)[c]	2.81	1.83	0.75	0.95	8.28	2.18	0.59	2.46
μ_{ES}(D)[d]	2.90	1.89	0.95	1.04	8.73	2.22	0.88	2.12
$\Delta\mu$(D)	0.09	0.06	0.20	0.09	0.45	0.04	0.29	-0.34
HOMO(eV)	-5.94	-5.90	-5.72	-5.85	-6.04	-5.96	-5.81	-5.91
LUMO(eV)	-3.41	-3.42	-3.24	-3.52	-3.44	-3.40	-3.27	-3.51
Optical bandgap (eV)	1.93	1.88	1.88	1.77	1.98	1.94	1.94	1.83
Electronic bandgap (eV)	2.53	2.48	2.48	2.33	2.60	2.56	2.54	2.40

a) oscillator strength; b) contribution of the HOMO-LUMO transition to the overall ground state-first excited state transition; c) dipole moment in the ground state; d) dipole moment in the first excited state.

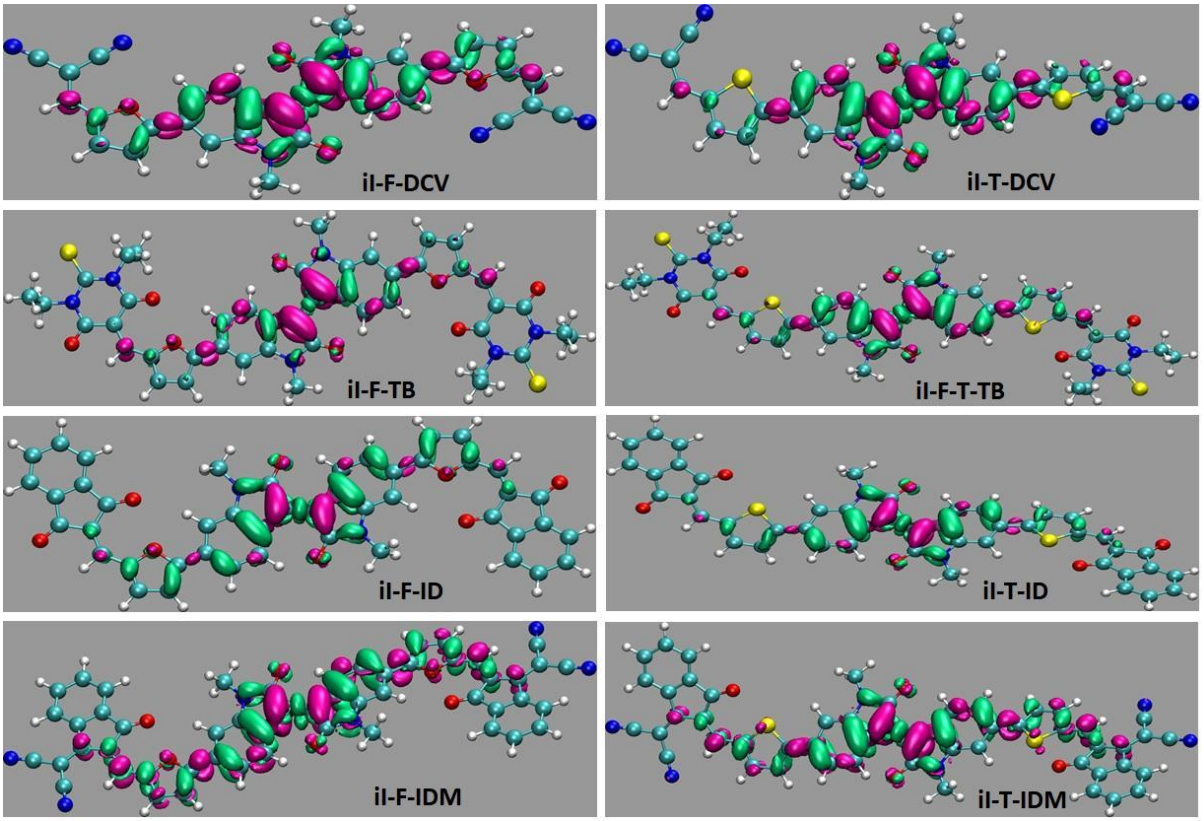

Figure 5. Total electron density difference plots (see text). Magenta: negative; green: positive; the density isovalues of the pictures correspond to 11% of the total electron density of each molecule

3.5. Optical, electro-chemical and structural characterization of dye's thin films

Different characterizations have been performed on the dyes processed as thin films by spin coating or drop casting procedures. For what concerns the optical properties, thin films of the dyes have been prepared by spin coating from $CHCl_3$-TCE solution (95-5 % v/v); the films were then annealed at 120 °C for 1 h and their absorption spectra are shown in Figure 6. The annealing procedure generally provided, as compared to the as prepared films, a red shift of the absorption peaks (see Figures S33-S34) suggesting an increased structuration of dyes (with the exception of **iI-T-DCV** and **iI-T-IDM** that does not significantly change their optical features upon annealing). The same annealing procedure was employed in the OFETs fabrication as discussed below.

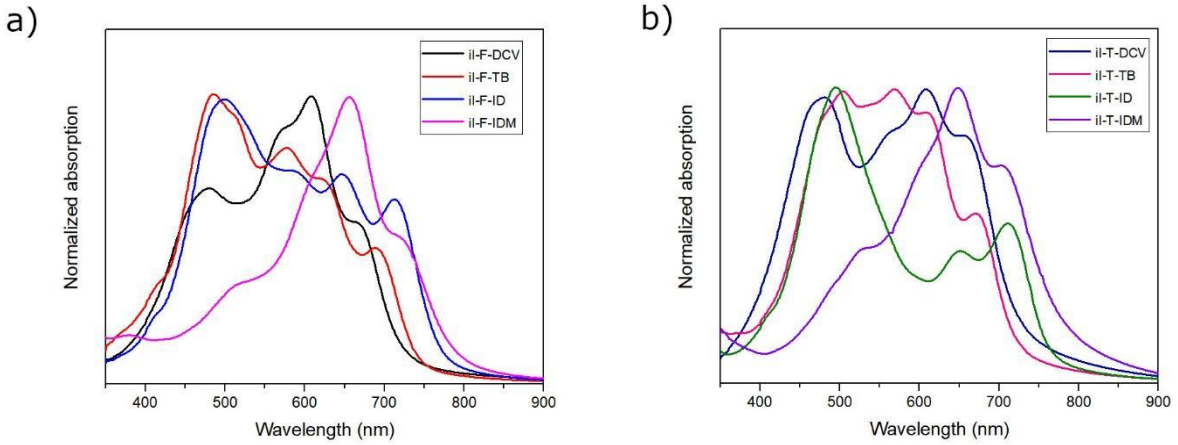

Figure 6. Optical spectra of the synthesized dyes as thin films spin coated from $CHCl_3$-TCE solution (95-5 v-v) and annealed at 120 °C for 1h.

As compared to the behaviour in solution, a clear red shift of the optical absorption is observed, indicating a significant π-π intermolecular interaction occurring in the solid state. As for the solution, two main optical features in the visible are present, the first one at around 500 nm and the second one occurring at higher wavelengths (600-700 nm) and characterized by a vibronic structure. For **IDM**-terminated series the absorption at longer wavelengths significantly prevails over the absorption at around 500 nm; the opposite behaviour is instead shown by **iI-T-ID** dye. All the other dyes show a broad absorption in all the visible spectrum with a full width at half maximum (FWHM) exceeding 200 nm (see Table 2). In particular **iI-F-ID**, **iI-T-DCV** and **iI-T-TB** dyes present a significant absorption in almost all the visible part of the spectrum. Optical bandgap of the dye's thin film was graphically determined by means of Tauc's Plot methodology.[41] All the molecules feature a narrow optical bandgap with values approaching 1.60 eV for **IDM** terminated dyes (see Table 4). Tauc's plot are reported in Figure S35-42.

Table 4. Optical properties of dye's thin films prepared by spin coating

Dyes	λ_1(nm)	λ_2(nm)	λ_3(nm)	λ_4(nm)	FWHM (nm)[a]	E_g(eV)[b]
iI-F-DCV	478	573	608	664	242	1.76
iI-F-TB	485	578	620	689	213	1.71
iI-F-ID	499	585	647	712	285	1.65
iI-F-IDM	516	-	657	718	146	1.61
iI-T-DCV	480	570	608	657	269	1.77
iI-T-TB	504	569	609	672	242	1.75
iI-T-ID	496	-	651	711	115	1.66
iI-T-IDM	532	-	649	704	176	1.60

a) Wavelength range with absorbance higher than half value of the absorption maxima; b) determined by Tauc's Plot methodology.[41]

The dyes were electrochemically characterized by means of cyclic voltammetry. Electrochemical experiments were performed on the dyes drop casted as thin films on a gold working electrode from DCM solution in a three-electrode set-up, as described in the Experimental Section. The recorded voltammograms are shown in Figure 7. All the samples show quasi reversible oxidation peaks in the oxidation scan except **iI-F-DCV and iI-F-IDM** which are characterized by an irreversible oxidation phenomenon. For sake of homogeneity, for all the samples we chose to report the oxidation potential as the voltage value corresponding to the onset of the oxidation (see Table 5). By reporting the potentials relative to the ferrocene/ferrocenium couple, it is possible to obtain the energies values of HOMO (associated with the oxidation potential) by applying the following relation[42]:

$$E_{HOMO}(eV) = -\left(E^{ox}_{onset} + 5.1\right)eV \quad (2)$$

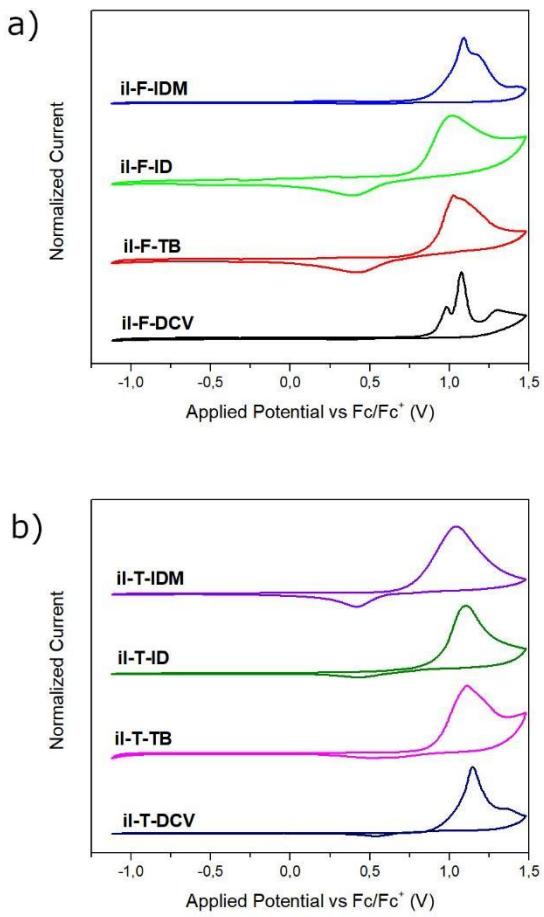

Figure 7. CV graphs of the reported dyes as drop casted films: a) F-series; b) T-series. A dye-covered Pt disk, a Pt wire and Ag/AgCl(3M) are used as working, counter and reference electrodes, respectively. Scan speed = 100 mV/s in 0.1 M solution of hexafluorophosphate in anhydrous acetonitrile

All the dyes are characterized by a stable HOMO energy, consistently with the good thermo-oxidative stability emerged by thermogravimetric analysis. Regarding LUMO energies, values around -4.3 eV and lower are found and suggest potential n-type behaviour for all the synthesized organic semiconductors. A direct comparation with difuryl-DPP derivatives previously reported[21] can be done: as already observed in the literature, replacing the difuryl-DPP core with

iI, lead to a significant stabilization of both HOMO and LUMO (with the only exception of **iI-F-IDM** LUMO which keeps almost the same value of the analogous DPP derivative).

Table 5: Electrochemical properties of the studied dyes as thin films

Dyes	Oxidation onset (V)[a]	HOMO[b]	LUMO (eV)[c]
iI-F-DCV	0.90	-6.00	-4.28
iI-F-TB	0.86	-5.96	-4.27
iI-F-ID	0.80	-5.90	-4.33
iI-F-IDM	0.93	-6.03	-4.27
iI-T-DCV	0.95	-6.05	-4.24
iI-T-TB	0.92	-6.02	-4.25
iI-T-ID	0.89	-5.99	-4.25
iI-T-IDM	0.77	-5.87	-4.42

a) Oxidation potentials were calculated vs ferrocenium/ferrocene couple; b) HOMO energies were determined from oxidation potentials according to reference [42]; c) LUMO energies were calculated by adding HOMO energy and the experimentally determined optical bandgap.

X-ray diffraction spectra were recorded on drop-casted films of the dyes deposed by chloroform solution on glass substrate (coverslip microscope glasses). After deposition, the thin films were thermally annealed at 120 °C for one hour in a vacuum oven. XRD patterns are shown in Figure 8. All the dyes are characterized by a strong and sharp diffraction peak at low 2θ values (100), accompanied in almost all the cases, by smaller peaks corresponding to higher order reflections of

the first one. This pattern is indicative of a lamellar organization with the inter-lamellar distance dictated by the length of the functionalizing alkyl chain. Interestingly, even if all the dyes are functionalized with the same 2-octyldodecyl alkyl chains, the position of the above-mentioned peak (and hence, the inter-lamellar distance) is clearly influenced by the auxiliary acceptor end groups: an interlamellar distance of ~21, 25, 24 and 16 Å were found, respectively for **DCV**, **TB**, **ID** and **IDM** functionalized dyes of both F and T series. This difference could be associated to a different degree of interdigitation of the branched alkyl chain functionalizing the dyes on the isoindigo nitrogen. In the case of **DCV** terminated dyes (Figure 8 a and b) a clear diffraction peak is observed also at ~25 °, indicative of a strong π-π interaction corresponding to a stacking distance of 3.50 Å. The same π-π stacking arrangement is expected to be present in all the dyes although it is not visible in the XRD patterns of **TB**, **ID** and **IDM** functionalized dyes probably because of an iso-orientation of the crystals on the glass surface.

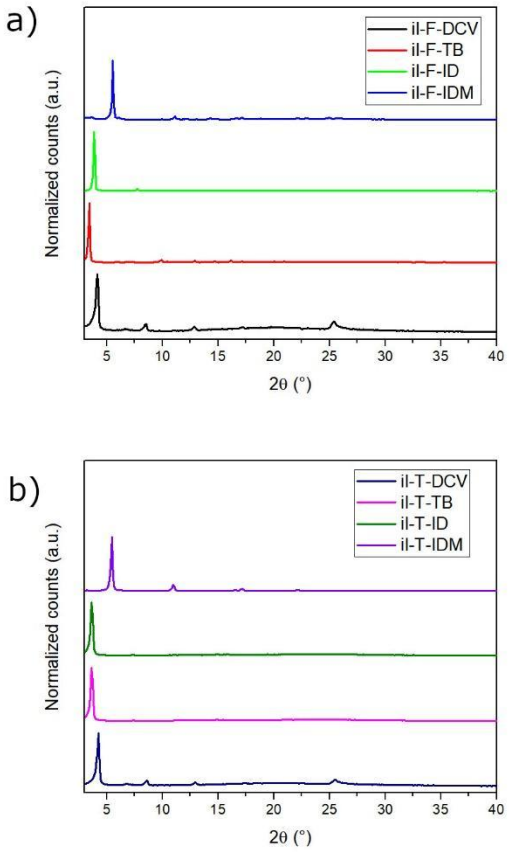

Figure 8. XRD spectra for the drop-casted films of the synthesized dyes: a) F-Series; b) T-Series

3.6. Electrical characterization

All the field-effect transistors featuring spin-coated active channels based on the dyes investigated in this study were found to display a pure n-type response (electron accumulation) with the I_{DS} current enhancement observable only under the application of positive V_{GS} voltages.

Figure 9a and 9b, in particular, show the output curves measured for the **il-F-ID** and **il-T-DCV** compounds, while the corresponding transfer curves are reported in Figure 9c. For sake of completeness, analogous curves are reported for the remaining compounds in the Figures S43 and S34 (see the Supplementary File).

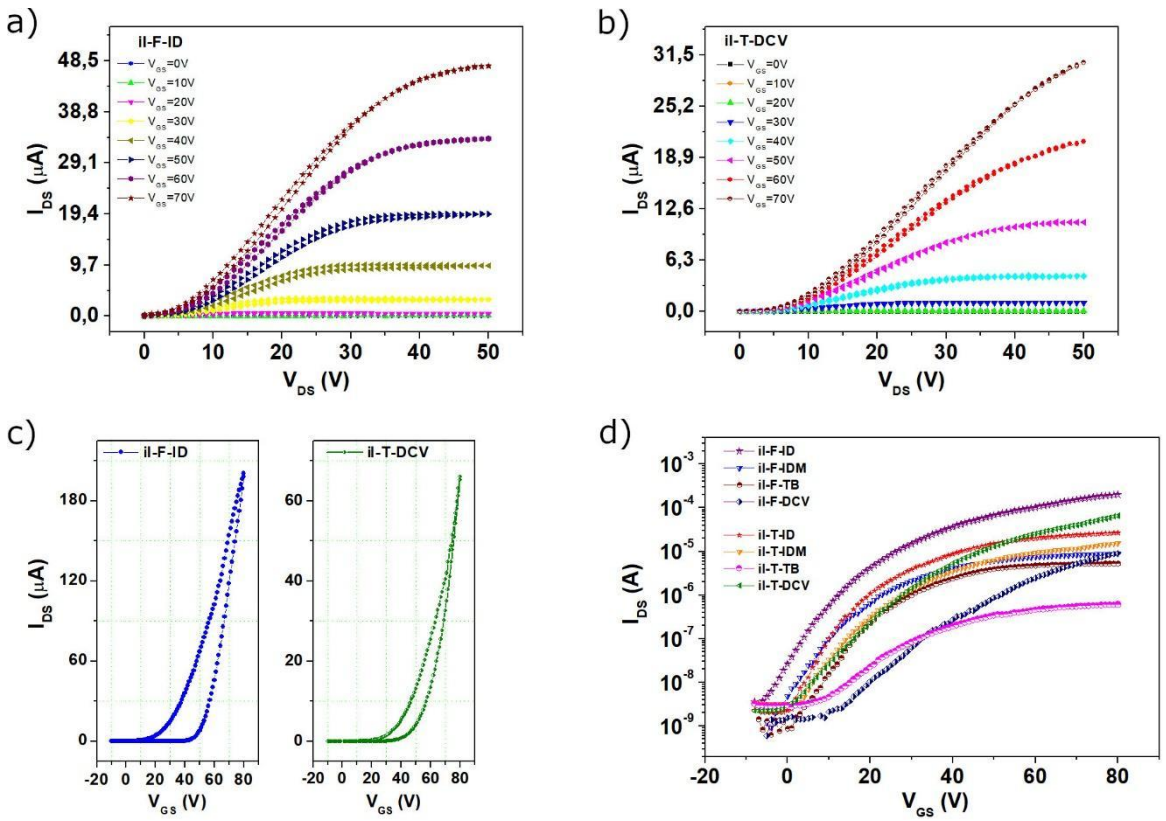

Figure 9. Output curves measured for transistors based on a) **iI-F-ID** and b) **iI-T-DCV** molecules. c) Corresponding transfer-curves recorded in the saturation regime (V_{DS}=+50V) for the same compounds. d) Semi-log plot of a set of transfer curves measured in saturation regime for all the investigated compounds. Here, only the forward scans are shown for sake of clarity.

The transfer curves reveal more clearly the occurrence of hysteresis effects with the current values measured in the forward sweep (from the off to the on region) being larger than those measured in the backward (from the on to the off regions) sweep. This phenomenon is classically associated to the action of the trapping mechanisms which tend to immobilize the charge carriers and reduce progressively their charge density throughout the measurement. [43] On the other hand, the general diode-like response observed in the low V_{DS} region of the output curves seems to suggest a non-negligible contribution of the contact-resistance (R_C) effect, also this being a common feature for bottom-contact organic transistors where effects related to the active channel morphology-near the source/drain contacts become dominant. [44]

Figure 9d offers a more compact view of the performed electrical tests with a set of transfer curves (one for each compound) plotted in a semi-log graph. From these, it is possible to infer the superior behaviour of the **iI-F-ID** compound, while **iI-T-TB** seems the material displaying by far the lowest current values. The overall transistors performances, evaluated in terms of field-effect mobility and threshold voltage values, are more exhaustively summarized in Table 6. It should be outlined that, here, as commonly reported in literature,[45] only the current curves recorded in the forward sweep were considered for the parameter estimation.

Table 6 confirms the distinctive behaviour of **iI-F-ID** being the only compound with an average mobility exceeding 10^{-2} $cm^2/V \cdot s$. Conversely, **iI-T-TB** is the dye with the worst electrical response ($\mu_e^{ave} < 10^{-4}$ $cm^2/V \cdot s$). All the remaining molecules exhibit mobility values around 10^{-3} $cm^2/V \cdot s$, with the exception of **iI-T-DCV** for which the average mobility overcomes $3.5 \cdot 10^{-3}$ $cm^2/V \cdot s$.

For all the compounds, the threshold voltages are significantly larger than 0 V but no clear correlation could be identified with mobility. **iI-F-ID** and **iI-T-TB**, for instance, show similar V_{th} values despite the remarkable differences in terms of their mobility values).

At this stage, the reason for the distinctive electron mobility performances of **iI-F-ID** as compared to the other dyes could be ascribed to the combination of a particularly stable LUMO (the experimental LUMO energy, -4.33 eV, is the lower among all the dyes apart from **iI-T-IDM**) with a significant tendency to highly ordered organization in the solid phase. This latter feature can be extrapolated from the very pronounced vibronic structuration observed in the film's UV-Vis spectrum and from XRD spectrum, showing a very sharp main diffraction peak, being significantly larger in comparison with that exhibited by the other dyes.

Table 6. Electron mobility (μ) and threshold voltage (V_{th}) values estimated by Eq.1 for the OFET based on the investigated dyes. The average values were achieved considering at least 4 different devices for any compound.

Dyes	μ_e^{aver} ($cm^2/V \cdot s$) $\cdot 10^{-3}$	μ_e^{max} ($cm^2/V \cdot s$) $\cdot 10^{-3}$	$V_{th,e}^{Avg}$ (V)
iI-F-DCV	*0.65±0.40*	*1.27*	*35.3±1.2*
iI-F-TB	*0.91±0.62*	*1.62*	*20.3 ±8.8*
iI-F-ID	*10.7±1.7*	*11.9*	*13.6±2.9*
iI-F-IDM	*0.91±0.18*	*1.10*	*13.6 ± 8.9*
iI-T-DCV	*3.59±0.79*	*4.46*	*27.4±5.6*
iI-T-TB	*0.046±0.007*	*0.055*	*11.6±4.7*
iI-T-ID	*1.69±0.24*	*1.98*	*9.8±0.7*
iI-T-IDM	*1.34±0.6*	*2.24*	*20.0±1.6*

Finally, for the sake of completeness, morphological features of the deposited active layers were investigated by non-contact AFM as shown in Figure S35 where film surface topographies are reported. These images suggest a reduced granular character of the **iI-F-ID** and **iI-T-DCV** layers as a consequence of the presence of larger crystallites and coherently with the improved charge transport features exhibited by these two dyes.

4. Conclusions and perspectives

We report here on the synthesis and characterization of eight novel isoindigo (**iI**) derivatives. The dyes are characterized by **iI** electron acceptor core symmetrically coupled by two donor

heteroaromatics (furan in F-series and tiophene in T-series) and end-functionalized with EWGs of different strength. The dyes are characterized by a very high thermal stability with decomposition temperature, in air, ranging from 360 to 400 °C. A careful computational study, performed at DFT level, revealed some interesting properties about the electronic structure of the dyes. Upon photoexcitation, a transfer of electron density occurs in a direction that is dependent on the specific EWG considered: for **IDM** and **DCV** acceptor, and, in a minor extent, for **TB**, electron density moves toward the periphery of the dye. The opposite occurs when considering **ID** acceptor, with the electron density moving toward the core of the molecules. Optical spectra recorded in chloroform solution show a clear dependence of the absorption maxima wavelengths from the strength of the terminal EWGs: the higher the latter, the more red-shifted the former. Optical characterization was performed on thin films as well: in the solid state a significant red shift of the absorption, as compared to solution, occurs along with a vibronic structuration of the peaks. This behaviour is clearly associated to the strong intermolecular interactions taking place in the crystalline phase. All the dyes are characterized, in the solid state, by a narrow bandgap approaching 1.6 eV for the indandione substituted dyes. Another appealing property of the dyes in film phase, is a diffuse absorption along the visible part of the spectrum, with a full width at half maximum (FWHM) exceeding 200 nm for six out of the eight dyes. XRD analysis performed on thin films of the dyes, show a lamellar organization; interestingly, the width of these lamellae is related to the nature of the terminal EWG and independent from the donor heteroaromatics. The dyes were moreover characterized electro-chemically to determine HOMO and LUMO energies: very stable LUMO energies were found, around or lower than -4.3 eV. Stable HOMO (around -6 eV) were found, consistently with the high thermo-oxidative stability exhibited by the dyes. The dyes were moreover studied as active layers in OFET to investigate their charge transport properties: unipolar n-type behaviour was observed for all the dyes. Electron mobility in the order of 10^{-2}

$cm^2/V{\cdot}s$ was found for **iI-F-ID** dye while for the other compounds the same parameter was found to be lowered by about one order of magnitude. The higher mobility value of **iI-F-ID** could be ascribed to a particular stable LUMO along with a higher tendency to crystallize. Further studies about the crystal packing of these dyes will be carried out in the next future to better elucidate structure-properties relationships. The novel isoindigo dyes here reported emerge as promising materials in different field of solar light driven applications. Their ability to diffusely absorb in the visible spectrum, their good electron-mobility and a proper FMOs energy alignment with the most efficient donor polymers in bulk heterojunction organic solar cells,[46,47] suggest they can be efficiently used as nonfullerene (NFA) acceptors: the ease of synthesis as compared the most performant NFA fused systems[48,49] represents a further element of interest in this class of materials. In addition, due to their n-type charge transport behaviour and the peculiar opto-electronic features along with their nice filmability, these two series of isoindigo dyes could be exploited as electron transport materials (ETM) in Perovskite Solar Cells (PSc).[50,51] Indeed, LUMO energy level of the dyes is only slightly upshifted compared to the conventional organic ETM (e.g. PCBM) whereas HOMO energy level are enough deep to avoid unwanted recombination. Their insolubility in the solvents (DMF, DMSO) typically used for MAPI deposition in PSc, could, moreover, help the processing of this kind of multilayer device. Finally, the long and branched alkyl tails of the here reported dyes, could help their self-assembled as nanoparticles by hydrophobic effect and can be exploited to realize, in combination with donor polymers, photocatalytic nano-heterojunctions for hydrogen production in what is one of the most recent and appealing applications of organic semiconductors blends.[52,53]

Acknowledgements

The national project PON E-Design (ARS01_01158), funded by the Italian Ministry of Education, University and Research (MIUR) and the Project FRA 2021 “MEREMOC”, funded by University of

Naples Federico II are acknowledged. CPU computing time was granted by the “Departments of Excellence-2018” Program (Dipartimenti di Eccellenza) of the Italian Ministry of Research, DIBAF-Department of University of Tuscia, Project “Landscape 4.0 - food, wellbeing and environment” (Prof. Nico Sanna).

References

[1] Gsänger M, Bialas D, Huang L, Stolte M, Würthner F. Organic Semiconductors based on Dyes and Color Pigments. Advanced Materials 2016;28:3615–45. https://doi.org/10.1002/ADMA.201505440.

[2] Li C, Wonneberger H. Perylene Imides for Organic Photovoltaics: Yesterday, Today, and Tomorrow. Advanced Materials 2012;24:613–36. https://doi.org/10.1002/ADMA.201104447.

[3] Zhan X, Facchetti A, Barlow S, Marks TJ, Ratner MA, Wasielewski MR, et al. Rylene and Related Diimides for Organic Electronics. Advanced Materials 2011;23:268–84. https://doi.org/10.1002/ADMA.201001402.

[4] Hendsbee AD, Sun JP, Rutledge LR, Hill IG, Welch GC. Electron deficient diketopyrrolopyrrole dyes for organic electronics: synthesis by direct arylation, optoelectronic characterization, and charge carrier mobility. J Mater Chem A Mater 2014;2:4198–207. https://doi.org/10.1039/C3TA14414C.

[5] Li Y, Sonar P, Murphy L, Hong W. High mobility diketopyrrolopyrrole (DPP)-based organic semiconductor materials for organic thin film transistors and photovoltaics. Energy Environ Sci 2013;6:1684. https://doi.org/10.1039/c3ee00015j.

[6] Tang A, Zhan C, Yao J, Zhou E. Design of Diketopyrrolopyrrole (DPP)-Based Small Molecules for Organic-Solar-Cell Applications. Advanced Materials 2017;29. https://doi.org/10.1002/adma.201600013.

[7] Hunger Klaus. Industrial Dyes: Chemistry, Properties, Applications Edited by Klaus Hunger (Kelkheim, Germany). Wiley-VCH: Weinheim. 2003. xxiv + 600 pp. $185.00. ISBN 3-527-30426-6. J Am Chem Soc 2003;125:10144–10144. https://doi.org/10.1021/ja0335418.

[8] Głowacki ED, Voss G, Sariciftci NS. 25th Anniversary Article: Progress in Chemistry and Applications of Functional Indigos for Organic Electronics. Advanced Materials 2013;25:6783–800. https://doi.org/10.1002/ADMA.201302652.

[9] Wei X, Zhang W, Yu G. Semiconducting Polymers Based on Isoindigo and Its Derivatives: Synthetic Tactics, Structural Modifications, and Applications. Adv Funct Mater 2021;31:2010979. https://doi.org/10.1002/ADFM.202010979.

[10] Li JL, Cao JJ, Duan LL, Zhang HL. Evolution of Isoindigo-Based Electron-Deficient Units for Organic Electronics: From Natural Dyes to Organic Semiconductors. Asian J Org Chem 2018;7:2147–60. https://doi.org/10.1002/AJOC.201800198.

[11] Wang E, Mammo W, Andersson MR, Wang E, Andersson MR, Mammo W. 25th Anniversary Article: Isoindigo-Based Polymers and Small Molecules for Bulk Heterojunction Solar Cells and Field Effect Transistors. Advanced Materials 2014;26:1801–26. https://doi.org/10.1002/ADMA.201304945.

[12] Stalder R, Mei J, Graham KR, Estrada LA, Reynolds JR. Isoindigo, a versatile electron-deficient unit for high-performance organic electronics. Chemistry of Materials 2014;26:664–78. https://doi.org/10.1021/CM402219V/ASSET/IMAGES/CM402219V.SOCIAL.JPEG_V03.

[13] Liao SF, Lu CF, Fenta AD, Chen CT, Chao CY, Su WF. High face-on ratio isoindigo copolymers with extended nano-fibrillar networks in fullerene-based thick (>300 nm) photovoltaics achieving a high efficiency of 10.7%. J Mater Chem A Mater 2019;7:21309–20. https://doi.org/10.1039/C9TA06719A.

[14] Zhu L, Wang M, Li B, Jiang C, Li Q. High efficiency organic photovoltaic devices based on isoindigo conjugated polymers with a thieno[3,2-b]thiophene π-bridge. J Mater Chem A Mater 2016;4:16064–72. https://doi.org/10.1039/C6TA07138D.

[15] Jung EH, Ahn H, Jo WH, Jo JW, Jung JW. Isoindigo-based conjugated polymer for high-performance organic solar cell with a high VOC of 1.06 V as processed from non-halogenated solvent. Dyes and Pigments 2019;161:113–8. https://doi.org/10.1016/J.DYEPIG.2018.09.048.

[16] Lei T, Wang JY, Pei J. Design, synthesis, and structure-property relationships of isoindigo-based conjugated polymers. Acc Chem Res 2014;47:1117–26. https://doi.org/10.1021/AR400254J/ASSET/IMAGES/AR400254J.SOCIAL.JPEG_V03.

[17] Lei T, Cao Y, Fan Y, Liu CJ, Yuan SC, Pei J. High-performance air-stable organic field-effect transistors: Isoindigo-based conjugated polymers. J Am Chem Soc 2011;133:6099–101. https://doi.org/10.1021/JA111066R/SUPPL_FILE/JA111066R_SI_001.PDF.

[18] Meng B, Ren Y, Liu J, Jäkle F, Wang L. p–π Conjugated Polymers Based on Stable Triarylborane with n-Type Behavior in Optoelectronic Devices. Angewandte Chemie International Edition 2018;57:2183–7. https://doi.org/10.1002/ANIE.201712598.

[19] Roncali J, Leriche P, Blanchard P. Molecular Materials for Organic Photovoltaics: Small is Beautiful. Advanced Materials 2014;26:3821–38. https://doi.org/10.1002/ADMA.201305999.

[20] Mishra A, Bäuerle P, Mishra A, Bäuerle P. Small Molecule Organic Semiconductors on the Move: Promises for Future Solar Energy Technology. Angewandte Chemie International Edition 2012;51:2020–67. https://doi.org/10.1002/ANIE.201102326.

[21] Fusco S, Barra M, Bonomo M, Cassinese A, Centore R, Chiarella F, et al. Novel DPP derivatives functionalized with auxiliary electron-acceptor groups and characterized by narrow bandgap and ambipolar charge transport properties. Dyes and Pigments 2021;186:109026. https://doi.org/10.1016/j.dyepig.2020.109026.

[22] Fusco S, Barra M, Gontrani L, Bonomo M, Chianese F, Galliano S, et al. Novel Thienyl DPP derivatives Functionalized with Terminal Electron-Acceptor Groups: Synthesis, Optical Properties and OFET Performance. Chemistry – A European Journal 2022;28:e202104552. https://doi.org/10.1002/CHEM.202104552.

[23] Maglione C, Carella A, Centore R, Fusco S, Velardo A, Peluso A, et al. Tuning optical absorption in pyran derivatives for DSSC. J Photochem Photobiol A Chem 2016;321:79–89. https://doi.org/10.1016/j.jphotochem.2016.01.018.

[24] Maglione C, Carella A, Carbonara C, Centore R, Fusco S, Velardo A, et al. Novel pyran based dyes for application in dye sensitized solar cells. Dyes and Pigments 2016;133:395–405. https://doi.org/10.1016/j.dyepig.2016.06.024.

[25] Li S, Yuan J, Deng P, Ma W, Zhang Q. A comparative study of diketopyrrolopyrrole and isoindigo based polymers for organic photovoltaic applications. Dyes and Pigments 2014;106:121–7. https://doi.org/10.1016/J.DYEPIG.2014.03.002.

[26] He M, Li W, Gao Y, Tian H, Zhang J, Tong H, et al. Donor–Acceptor Conjugated Polymers Based on Dithieno[3,2-b:3′,2′-b′]naphtho[1,2-b:5,6-b′]dithiophene: Synthesis and Semiconducting Properties 2016. https://doi.org/10.1021/ACS.MACROMOL.5B02583.

[27] Zhang G, Fu Y, Xie Z, Zhang Q. Synthesis and photovoltaic properties of new low bandgap isoindigo-based conjugated polymers. Macromolecules 2011;44:1414–20. https://doi.org/10.1021/MA102357B/SUPPL_FILE/MA102357B_SI_001.PDF.

[28] Yanai T, Tew DP, Handy NC. A new hybrid exchange-correlation functional using the Coulomb-attenuating method (CAM-B3LYP). Chem Phys Lett 2004;393:51–7. https://doi.org/10.1016/j.cplett.2004.06.011.

[29] Adamo C, Barone V. Toward reliable density functional methods without adjustable parameters: The PBE0 model. Journal of Chemical Physics 1999;110:6158–70. https://doi.org/10.1063/1.478522.

[30] Zhao Y, Truhlar DG. The M06 suite of density functionals for main group thermochemistry, thermochemical kinetics, noncovalent interactions, excited states, and transition elements: Two new functionals and systematic testing of four M06-class functionals and 12 other function. Theor Chem Acc 2008;120:215–41. https://doi.org/10.1007/s00214-007-0310-x.

[31] Tomasi J, Mennucci B, Cancès E. The IEF version of the PCM solvation method: an overview of a new method addressed to study molecular solutes at the QM ab initio level. Journal of Molecular Structure: THEOCHEM 1999;464:211–26. https://doi.org/10.1016/S0166-1280(98)00553-3.

[32] Frisch MJ et al. Gaussian 16, Revision A.03 2016.

[33] Gontrani L, Mennucci B, Tomasi J. Glycine and alanine: a theoretical study of solvent effects upon energetics and molecular response properties. Journal of Molecular Structure: THEOCHEM 2000;500:113–27. https://doi.org/10.1016/S0166-1280(00)00390-0.

[34] Schlegel HB. Optimization of equilibrium geometries and transition structures. J Comput Chem 1982;3:214–8. https://doi.org/10.1002/jcc.540030212.

[35] O'Boyle NM, Tenderholt AL, Langner KM. cclib: A library for package-independent computational chemistry algorithms. J Comput Chem 2008;29:839–45. https://doi.org/10.1002/JCC.20823.

[36] Dennington R, Keith TA, Millam JM. GaussView, Version 6 2016.

[37] Chiarella F, Chianese F, Barra M, Parlato L, Toccoli T, Cassinese A. Spontaneous wetting dynamics in perylene diimide n-type thin films deposited at room temperature by supersonic molecular beam. Journal of Physical Chemistry C 2016;120:26076–82. https://doi.org/10.1021/ACS.JPCC.6B07310/ASSET/IMAGES/LARGE/JP-2016-073102_0003.JPEG.

[38] Bloisi F, Pezzella A, Barra M, Alfè M, Chiarella F, Cassinese A, et al. Effect of substrate temperature on MAPLE deposition of synthetic eumelanin films. Appl Phys A Mater Sci Process 2011;105:619–27. https://doi.org/10.1007/s00339-011-6603-x.

[39] Kim J, Song CE, Lee SK, Lim E. Synthesis and characterization of small molecules with isoindigo substituted dye end groups. J Nanosci Nanotechnol 2016;16:8737–40. https://doi.org/10.1166/JNN.2016.12526.

[40] Martin RL. Natural transition orbitals. Journal of Chemical Physics 2003;118:4775–7. https://doi.org/10.1063/1.1558471.

[41] Coluccini C, Manfredi N, Salamone MM, Ruffo R, Lobello MG, de Angelis F, et al. Quaterpyridine ligands for panchromatic Ru(II) dye sensitizers. Journal of Organic Chemistry 2012;77:7945–56. https://doi.org/10.1021/jo301226z.

[42] Cardona CM, Li W, Kaifer AE, Stockdale D, Bazan GC. Electrochemical considerations for determining absolute frontier orbital energy levels of conjugated polymers for solar cell applications. Advanced Materials 2011;23:2367–71. https://doi.org/10.1002/adma.201004554.

[43] Chiarella F, Barra M, Ricciotti L, Aloisio A, Cassinese A. Morphology, electrical performance and potentiometry of PDIF-CN2 thin-film transistors on hmds-treated and bare silicon dioxide. Electronics (Switzerland) 2014;3:76–86. https://doi.org/10.3390/electronics3010076.

[44] Chianese F, Chiarella F, Barra M, Candini A, Affronte M, Cassinese A. Suppression of the morphology mismatch at graphene/n-type organic semiconductor interfaces: a scanning Kelvin probe force microscopy investigation. J Mater Chem C Mater 2020;8:8145–54. https://doi.org/10.1039/D0TC01099E.

[45] Xu Y, Li Y, Li S, Balestra F, Ghibaudo G, Li W, et al. Precise Extraction of Charge Carrier Mobility for Organic Transistors. Adv Funct Mater 2020;30:1904508. https://doi.org/10.1002/ADFM.201904508.

[46] Zheng Z, Yao H, Ye L, Xu Y, Zhang S, Hou J. PBDB-T and its derivatives: A family of polymer donors enables over 17% efficiency in organic photovoltaics. Materials Today 2020;35:115–30. https://doi.org/10.1016/J.MATTOD.2019.10.023.

[47] Zheng B, Huo L, Li Y. Benzodithiophenedione-based polymers: recent advances in organic photovoltaics. NPG Asia Materials 2020 12:1 2020;12:1–22. https://doi.org/10.1038/s41427-019-0163-5.

[48] Liu W, Xu X, Yuan J, Leclerc M, Zou Y, Li Y. Low-Bandgap Non-fullerene Acceptors Enabling High-Performance Organic Solar Cells. ACS Energy Lett 2021;6:598–608. https://doi.org/10.1021/ACSENERGYLETT.0C02384/ASSET/IMAGES/LARGE/NZ0C02384_0004.JPEG.

[49] Li S, Li CZ, Shi M, Chen H. New Phase for Organic Solar Cell Research: Emergence of Y-Series Electron Acceptors and Their Perspectives. ACS Energy Lett 2020;5:1554–67. https://doi.org/10.1021/ACSENERGYLETT.0C00537/ASSET/IMAGES/LARGE/NZ0C00537_0005.JPEG.

[50] Zhang M, Zhan X, Zhang M, Zhan X. Nonfullerene n-Type Organic Semiconductors for Perovskite Solar Cells. Adv Energy Mater 2019;9:1900860. https://doi.org/10.1002/AENM.201900860.

[51] Wang D, Ye T, Zhang Y. Recent advances of non-fullerene organic electron transport materials in perovskite solar cells. J Mater Chem A Mater 2020;8:20819–48. https://doi.org/10.1039/D0TA06500E.

[52] Kosco J, Gonzalez-Carrero S, Howells CT, Fei T, Dong Y, Sougrat R, et al. Generation of long-lived charges in organic semiconductor heterojunction nanoparticles for efficient photocatalytic hydrogen evolution. Nature Energy 2022 7:4 2022;7:340–51. https://doi.org/10.1038/s41560-022-00990-2.

[53] Kosco J, Bidwell M, Cha H, Martin T, Howells CT, Sachs M, et al. Enhanced photocatalytic hydrogen evolution from organic semiconductor heterojunction nanoparticles. Nature Materials 2020 19:5 2020;19:559–65. https://doi.org/10.1038/s41563-019-0591-1.